HHS Public Access

Author manuscript

Annu Rev Vis Sci. Author manuscript; available in PMC 2022 September 15.

Published in final edited form as:

Annu Rev Vis Sci. 2021 September 15; 7: 693–726. doi:10.1146/annurev-vision-100419-111350.

Optical Coherence Tomography and Glaucoma

Alexi Geevarghese[1], **Gadi Wollstein**[1,2,3], **Hiroshi Ishikawa**[1,2], **Joel S. Schuman**[1,2,3,4]

[1]Department of Ophthalmology, NYU Langone Health, NYU Grossman School of Medicine, New York, NY 10016, USA

[2]Department of Biomedical Engineering, NYU Tandon School of Engineering, Brooklyn, New York 11201, USA

[3]Center for Neural Science, NYU College of Arts and Sciences, New York, NY 10003, USA

[4]Department of Physiology and Neuroscience, NYU Langone Health, NYU Grossman School of Medicine, New York, NY 10016, USA

Abstract

Early detection and monitoring are critical to the diagnosis and management of glaucoma, a progressive optic neuropathy that causes irreversible blindness. Optical coherence tomography (OCT) has become a commonly utilized imaging modality that aids in the detection and monitoring of structural glaucomatous damage. Since its inception in 1991, OCT has progressed through multiple iterations, from time-domain OCT, to spectral-domain OCT, to swept-source OCT, all of which have progressively improved the resolution and speed of scans. Even newer technological advancements and OCT applications, such as adaptive optics, visible-light OCT, and OCT-angiography, have enriched the use of OCT in the evaluation of glaucoma. This article reviews current commercial and state-of-the-art OCT technologies and analytic techniques in the context of their utility for glaucoma diagnosis and management, as well as promising future directions.

Keywords

glaucoma; optical coherence tomography; OCT; imaging

Joel.Schuman@nyu.edu .

DISCLOSURE STATEMENT

J.S.S. is an equity owner of, holds patents for, and receives royalties from Ocugenix. J.S.S. holds patents for, receives royalties from, and is a consultant/advisor for Carl Zeiss Meditec. J.S.S. is a consultant/advisor for and equity owner of Aerie Pharmaceuticals Inc., Ocular Therapeutix Inc., and Opticient. J.S.S. is a consultant/advisor for Boehringer Ingelheim, Perfuse Inc., Regeneron Inc., and SLACK Incorporated. J.S.S. receives grant support from the BrightFocus Foundation and the National Eye Institute. J.S.S. receives royalties for intellectual property licensed by the Massachusetts Eye and Ear Infirmary, Massachusetts Institute of Technology, and Tufts University. J.S.S., G.W., and H.I. receive royalties for intellectual property licensed by New York University and the University of Pittsburgh. A.G. is not aware of any affiliations, memberships, funding, or financial holdings that might be perceived as affecting the objectivity of this review.

INTRODUCTION

Glaucoma is a progressive optic neuropathy that is multifactorial and degenerative. It is characterized by the death of retinal ganglion cells (RGCs) and their axons, leading to characteristic optic disc and retinal nerve fiber layer (RNFL) structural changes and associated vision loss (Weinreb et al. 2016). Glaucoma is the leading cause of irreversible vision loss and the second leading cause of overall vision loss worldwide (Kapetanakis et al. 2016, Quigley & Broman 2006). Despite the progressive nature of glaucoma, existing effective treatments can slow or prevent further progression. Early detection and monitoring are critical to the management and preservation of vision and quality of life.

Important in the detection and management of glaucoma is optical coherence tomography (OCT) imaging. OCT was first introduced in 1991 by Huang et al. (1991) as a noninvasive in vivo cross-sectional imaging technology using low-coherence interferometry. OCT is the optical analogue of ultrasound imaging. It generates high-resolution cross-sectional 2D images of internal tissue microstructures. OCT was translated to clinical practice and became commercially available in 1996. The utility of OCT in the context of many ocular pathologies has been reported (Dong et al. 2016, Puliafito et al. 1995, Schuman et al. 1995). Specifically pertaining to glaucoma, OCT enables the quantitative evaluation of critical neural structures, including the RNFL, the optic nerve head (ONH), and the macula. OCT has revolutionized the diagnosis, monitoring, and ultimately management of glaucoma by taking glaucoma from a primarily subjectively assessed disease to an objectively evaluated disease. Significant iterative advances in OCT technology have happened since its inception, particularly improvements in resolution and scanning speed, which continue to impact glaucoma management.

Time-domain OCT (TD-OCT) (Figure 1) was the first generation of OCT. TD-OCT directs a near-IR (NIR) light at the retina and encodes the location of the back-reflected light based on time of flight by relating the reflection location to the position of a moving reference mirror (Dong et al. 2016). Limited by the maximal oscillating speed of the reference mirror, the top scanning speed of commercial TD-OCT was 400 axial scans/s (Hee et al. 1995, Kostanyan et al. 2015). In 2001, spectral-domain OCT (SD-OCT), also known as Fourier-domain OCT (FD-OCT), was introduced. In contrast to TD-OCT, SD-OCT evaluates the frequency spectrum of the interference between a stationary reference mirror and the reflected light, allowing spatial and structural information to be measured simultaneously at all echo time delays (axial pixels). The benefit of simultaneous assessment of all axial-depth scan (A-scan) pixels is the notable increase in scanning speed—up to 100,000 A-scans/s with commercial devices and even up to 20.8 million A-scans/s with research devices (Huber et al. 2006a,b, 2007; Potsaid et al. 2008; Wieser et al. 2010). In addition to the reduced acquisition time, SD-OCT has the advantage of increased signal-to-noise ratio (SNR), resulting in enhanced image quality (Choma et al. 2003, de Boer et al. 2003). Because scanning is so much faster, there can be fewer motion artifacts, and higher A-scan density can produce the illusion of higher transverse resolution when compared with TD-OCT. Furthermore, SD-OCT has a drop-off in SNR and axial resolution with increased distance from the zero-delay line (which appears as the top of the scan window). Image artifacts, such as those from segmentation errors, low signal quality, and media opacities

such as cataracts, occur with SD-OCT just as with TD-OCT (Hardin et al. 2015, Kostanyan et al. 2015, Leitgeb et al. 2003a, Yun et al. 2003).

Swept-source OCT (SS-OCT), another type of FD-OCT, allows for even faster scanning speeds of up to 200,000 A-scans/s with current commercial devices and in the millions of A-scans/s with laboratory devices. SS-OCT uses a laser that quickly sweeps through frequencies across a broad spectrum. The resulting interference pattern is captured by a photodetector; a spectrometer is not necessary. In contrast, SD-OCT instead uses a broad-bandwidth light source, and the interference pattern is captured by a spectrometer (Schuman 2008). SS-OCT permits high scan speeds (shorter scan speeds and higher scan density), less depth-dependent SNR and resolution drop-off, and improved scan quality (less eye movement). Most SS-OCT devices also use a center wavelength of approximately 1,050 nm (SD-OCT uses a center wavelength of approximately 850 nm), which allows for greater axial depth imaging and permits better visualization of deeper ophthalmologic structures such as the choroid and the lamina cribrosa (LC) (Adhi et al. 2014, Kostanyan et al. 2015, Mrejen & Spaide 2013).

OCT FOR GLAUCOMA DIAGNOSIS

The evaluation of glaucoma is highly dependent on the functional assessment of a patient's vision and the structural assessment of the retina and optic nerve. OCT was thus a major advance for glaucoma owing to the ability to visualize the retinal substructure. Automated segmentation of retinal layers allowed for objective quantification of retinal tissue layers, including the macula, peripapillary area, and the ONH. By comparing these measurements with established normative databases, clinicians can determine whether structures are borderline or outside normal limits, improving detection of disease and its progression. RNFL thinning is often one of the first signs of glaucoma, detectable often before changes in the visual field (Sommer et al. 1991). It has thus since become the most common clinical approach to detect and monitor glaucoma (Grewal & Tanna 2013, Schuman et al. 1995) (Figure 2). In addition to affecting circumpapillary RNFL, glaucoma preferentially affects the three innermost retinal layers of the macula, including the RNFL (which contains ganglion cell axons, neuroglia, and astrocytes), ganglion cell layer (which contains RGC bodies), and inner plexiform layer (IPL; which contains RGC dendrites, bipolar cell axons, and amacrine processes), which are collectively called the ganglion cell complex (GCC). Over half of all RGCs are located in the macula and are arranged in up to eight layers (Curcio & Allen 1990). Given that the RGC somata are 15–20 times the size of their axons and are in high density in the macula, abnormalities were thought to be more easily detectable in the macula than in the RNFL and thus to be of use for glaucoma diagnosis (Zeimer et al. 1998). Although this did not turn out to be so, glaucoma has been shown to cause macular RGC loss, and studies have shown significant differences when comparing macular thicknesses in glaucomatous eyes and healthy eyes (Guedes et al. 2003, Leung et al. 2005).

ONH and macular measurements with OCT have good reproducibility (Ghasia et al. 2015, Mwanza et al. 2010, Paunescu et al. 2004). Most studies have shown that SD-OCT and TD-OCT using RNFL have similar glaucoma discriminating ability (Bengtsson et al. 2012,

Jeoung & Park 2010, Schuman 2008, Sehi et al. 2009). SD-OCT is most commonly used, and many studies have reported good diagnostic capability of ONH parameters (disc area, rim area, cup-to-disc ratio, cup volume, RNFL thickness) and macular parameters [RNFL thickness, GCC thickness, ganglion cell–inner plexiform layer (GCIPL) minimum thickness, and GCIPL average thickness] for distinguishing glaucomatous eyes from glaucoma-suspect and healthy eyes with high areas under the receiver operating characteristic curve (AUCs), with better performance for more advanced disease (Bussel et al. 2014; Jeoung et al. 2013; Kotowski et al. 2012; Lisboa et al. 2013; Mwanza et al. 2011, 2012a; Sung et al. 2012a,c; Takayama et al. 2012). Evidence for the relative performance of ONH parameters has been conflicting. Some studies have demonstrated the superior performance of RNFL thickness compared with other ONH parameters, especially for detecting preperimetric glaucoma (Lisboa et al. 2013, Sung et al. 2012a), whereas other studies have demonstrated more comparable performance (Mwanza et al. 2011), which can be attributable to differences in disease severity. Total macular thickness, although significantly associated with glaucoma, has poor diagnostic performance compared with circumpapillary RNFL measurements (Greenfield et al. 2003, Wollstein et al. 2004). By quantifying individual layers within the macula on OCT scans, studies have shown that measurements of the GCIPL and the GCC had glaucoma discriminating performance comparable to that of circumpapillary RNFL and other ONH parameters, with minimum GCIPL performing superiorly to average and sectoral GCIPL (Jeoung et al. 2013, Kotowski et al. 2012, Mwanza et al. 2012a, Takayama et al. 2012). A meta-analysis by Oddone et al. (2016) concluded that average peripapillary RNFL is still more accurate than, although only slightly different from, macular parameters in diagnosing glaucoma. Diagnostic models that have incorporated multiple structural parameters were similar in performance but not superior to individual best-performing OCT parameters (Barella et al. 2013, Bizios et al. 2010, Grewal et al. 2008, Vidotti et al. 2013).

OCT FOR GLAUCOMA PROGRESSION

Once a patient is known to have glaucoma, assessment of disease progression is crucial. It can be challenging to distinguish perceived disease-related structural changes from intervisit measurement variability and normal age-related structural loss (Bussel et al. 2014, Leung et al. 2012). Detecting progression is critical for adjusting clinical management to prevent further RGC loss and functional loss. Although studies have shown that SD-OCT and TD-OCT using RNFL have similar glaucoma discriminating ability, SD-OCT has been reported to have increased sensitivity for detecting progression in RNFL (Bengtsson et al. 2012, Cho et al. 2011, Jeoung & Park 2010, Schuman 2008, Sehi et al. 2009). This can be explained by SD-OCT's high scan speed and image resolution, which can assess the retina with higher resolution while minimizing intervisit variability. Commercially available SD-OCT systems use algorithms to provide event-based analysis, trend-based analysis, or both for assessing progression (Figure 3). Event-based analysis identifies progression when a measurement exceeds an established threshold for change from baseline. Trend-based analysis assesses progression by evaluating the change of a parameter over time. Typically, progression is identified when the regression analysis of the parameter over time has a statistically significantly negative slope (i.e., the rate of change of the parameter). Although the trend-based analysis is less susceptible to outliers than event-based analysis, trend-based

analysis requires multiple tests to be reliable and may also be inappropriately assuming a linear relationship between measurements of structural damage and time (Bussel et al. 2014).

Although conclusions from existing studies are limited by the relatively short follow-up time within the context of a typically slowly progressive disease, studies thus far have demonstrated OCT is able to detect glaucoma progression with good sensitivity. One longitudinal study showed a greater likelihood of progression being detected by event analysis using TD-OCT scans compared with visual field testing (Wollstein et al. 2005). Subsequent studies have predominantly shown significant differences in the rate of change of RNFL in the group of glaucoma progressors as defined by optic disc photos, red-free RNFL photos, and visual field compared with the nonprogressor group (Na et al. 2013, Wessel et al. 2013). While some studies have shown similar progression detection sensitivity between RNFL and macula parameters of total macular thickness and GCIPL (Na et al. 2012), another study of a group of advanced glaucomatous eyes demonstrated the superior performance of average macular thickness loss, compared with the performance of RNFL or other parameters, in distinguishing progressors (Sung et al. 2012b). Another study has also shown that macular GCC global and focal loss volume outperforms ONH, RNFL thickness, and average GCC parameters in detecting progression (Naghizadeh et al. 2014). One study with a longer follow-up duration demonstrated superior sensitivity of OCT parameters, compared with visual field testing, for detecting progression in early glaucoma but not in more advanced stages. Additionally, the rate of RNFL thinning slowed dramatically in advanced glaucoma, thus diminishing its utility. However, the rate of GCC thinning remained relatively stable, allowing for sensitive progression detection even in advanced disease (X. Zhang et al. 2017).

Diagnosis and detection of progression can be complicated. For example, although myopia is a risk factor for glaucoma, it has also been linked to real structural changes as well as apparent artifactual changes that can be difficult to distinguish from true glaucomatous changes (Chang & Singh 2013, Mwanza et al. 2012b, Schuman 2016). The inclusion of a myopic normative database in OCT is one solution that can increase the specificity of diagnosis in patients with myopia, but the commercial implementation of this database has yet to be seen (Biswas et al. 2016). In the meantime, diagnosis in these populations should be approached with caution with close follow-up. As alluded to above, age-related changes affect both patients with glaucomatous eyes and patients with healthy eyes. The detection of progression should be done carefully to discriminate true glaucomatous progression from normal age-related changes, especially when evaluating the macula. Age effects have been observed to preferentially affect the macular parameters rather than circumpapillary parameters (Leung et al. 2013).

THE LAMINA CRIBROSA AS A BIOMARKER FOR GLAUCOMA

The LC is a fenestrated collagenous structure in the sclera of the eye through which RGC axons exit the eye to form the optic nerve. The LC is considered the primary site of RGC injury in glaucoma (Quigley et al. 1981). Notably, it is where both intracranial pressure and intraocular pressure exert effects simultaneously (Wang et al. 2017). It has been

proposed that one mechanism of injury in glaucoma is deformation of the beam and pore microstructure of the LC, leading to compression of axons, which blocks axonal transport, ultimately resulting in RGC death (Quigley & Anderson 1977, Radius & Anderson 1981, Sigal & Ethier 2009). Given the importance of the LC in glaucoma pathogenesis, the ability to image the LC is of interest. However, it is difficult to obtain adequate scans of deep structures such as the LC owing to high back-reflection from axons entering the ONH and the attenuation of signal as a function of the depth the light travels through tissue. Conventional ONH images acquired for RNFL thickness assessment yield a suboptimal view of the LC, as the LC lies posterior to the optic disc. In addition, the presence of large blood vessels and a thick prelaminar tissue (as is present in healthy subjects) further limits visibility of the LC. As a result, much research on the LC is dependent on histological examination and ex vivo modeling, but progress in OCT imaging has enabled in vivo examination of the LC. For one, postprocessing algorithms were developed that enhance SD-OCT signal contrast by compensating for light attenuation and reducing shadowing from blood vessels and peripapillary structures. Longer scanning times needed for imaging the LC increase vulnerability to motion artifacts from eye movements. Currently, there are OCT devices that incorporate eye-tracking technology and other software tools that can detect eye motion, discarding the resultant imaging artifact or correcting for eye motion (Girard et al. 2011, Mari et al. 2013, Sigal et al. 2014).

Enhanced-depth imaging (EDI) is an SD-OCT technique that improves the visualization of deeper structures such as the LC and the choroid. It was developed by Spaide et al. (2008) to visualize the full thickness of the choroid. With EDI, the SD-OCT device is brought close enough to the eye to use the inverted image of the fundus, placing the posterior-most portion of the image closest to the top of the scan window. Conventionally, the anterior-most structures are near the zero-delay line, at the top of the screen, where resolution and SNR are highest. This provides greater detail for this portion of the scan than for the deeper objects found farther down in the scan window. EDI results in a greater SNR and more robust evaluation of the LC. For example, EDI visualized the LC with higher reflectivity and contrast compared with conventional SD-OCT (Lee et al. 2011). EDI-OCT can demonstrate focal defects of the LC associated with local glaucomatous optic disc damage such as neuroretinal rim thinning/notching and acquired pits of the optic nerve (Kiumehr et al. 2012, You et al. 2013). Older commercial scanners with EDI-OCT did not offer high-density isotropic sampling of the LC, but averaged multiple frames to demonstrate deeper structures with the use of radial patterns or a wide distance between B-scans (cross-sectional tomographs) to minimize scan times (Lee et al. 2011, Nuyen et al. 2012, Sigal et al. 2014, Spaide et al. 2008, Takayama et al. 2013); however, newer software enables more useful scan patterns.

Compared with SD-OCT, SS-OCT has less reduction in sensitivity with increasing depths. SS-OCT's longer wavelengths and 3D raster scanning with high sampling density allow for better visualization of the LC (Nuyen et al. 2012, Sigal et al. 2014). Using this method, Wang et al. (2013) elucidated the 3D microstructure of the LC in the context of glaucoma. They found glaucomatous eyes had beam and pore microstructures significantly different from those in healthy eyes, potentially a consequence of structural remodeling and axonal loss (Figure 4).

ADAPTIVE OPTICS

Adaptive optics OCT (AO-OCT) is another important methodological advance in ophthalmic imaging that has improved resolution and scan quality. Originating from imaging protocols in the field of astronomy to reduce atmospheric distortion from diffraction, AO-OCT uses a deformable mirror to compensate for distortions from an incoming wavefront (Dong et al. 2017, Kostanyan et al. 2015, Lombardo et al. 2012). Optical aberrations of the eye can contribute to blurring and image artifacts in ophthalmic imaging, which AO technology aims to minimize (Charman & Chateau 2003, Godara et al. 2010, Guirao et al. 2002, Thibos et al. 2002, Williams 2011). Wavefront sensors developed in the 1990s allowed the measurement of low-order aberrations such as myopia, hyperopia, and astigmatism and high-order wavefront aberrations that occur in normal eyes (Castejón-Móchon et al. 2002, Diaz-Santana et al. 2003, Dong et al. 2017, Guirao et al. 2002, Lombardo et al. 2012, Nirmaier et al. 2003, Porter et al. 2001). AO technology is integrated with multiple ophthalmic imaging modalities. First, it was integrated with the conventional fundus camera in 1997, scanning laser ophthalmoscopy (SLO) in 2002, and OCT shortly thereafter in 2005. SD-OCT scan quality can be limited by the monochromatic aberrations of the eye, which impact the resolution of the images, but AO-OCT improves resolution substantially by compensating for these aberrations (Dong et al. 2017, Hermann et al. 2004, Hofer et al. 2001, Porter et al. 2001). Additionally, inherent to OCT are speckle artifacts that may obscure microscopic details, which AO helps reduce.

AO-OCT is capable of nearly diffraction-limited 3D resolution images of the ONH and retina, allowing the visualization of individual cells and photoreceptors (Dong et al. 2017). Researchers have been able to use AO coupled with a fundus camera, SLO, and OCT to assess the density of cone photoreceptors and the length of the inner and outer segments of cone photoreceptors (Choi et al. 2011). In one study, investigators demonstrate that in glaucoma initial changes in inner retinal thickness may be followed by outer retinal changes, including changes to the integrity and the density of cone photoreceptors in the outer retina that correlate with visual field sensitivity in the corresponding area. Photoreceptor outer segments were shorter with greater variability in retinal areas associated with visual field loss than in retinal areas that had no visual field loss or that were less affected (Kostanyan et al. 2015, Werner et al. 2011). AO-OCT can also reproducibly image RNFL axon bundles (Kocaoglu et al. 2011). This is useful because RGC axonal loss can precede structural changes of the ONH (Sommer et al. 1977, 1991) and functional changes detectable by standard automated perimetry. The ability to image at a microscopic level of resolution allows AO-OCT to map individual RNFL axon bundles in three dimensions and to further structurally differentiate healthy eyes from glaucomatous eyes (Kocaoglu et al. 2011, 2014; Torti et al. 2009). AO-OCT has also led to the observation that RNFL bundles exhibit a discrete reflectance pattern compared with surrounding tissue. Prior literature has suggested that the intensity of the reflectance pattern might decrease prior to RNFL thinning, offering another early sign of glaucomatous damage that is detectable with imaging (Huang et al. 2011b, Kocaoglu et al. 2011, van der Schoot et al. 2012, Zhang et al. 2011) but difficult to quantify owing to variability in measures of reflectance intensity, even normalizing to alternate structures in the OCT image. AO-OCT resolution has allowed increased

visualization of the LC and has been used to scan the LC in healthy, glaucoma-suspect, and glaucomatous eyes. A semiautomated segmentation analysis of 3D LC microstructure shows good measurement reproducibility (Dong et al. 2017, Nadler et al. 2014). Pairing AO with SS-OCT offers a promising avenue for future studies of the LC (Jian et al. 2016).

AO-OCT and other imaging modalities have been combined in a way that takes advantage of the strengths of these different imaging modalities. AO-SLO allows for high transverse resolution, short scanning times, and direct measurements of back-reflected light intensity. AO-OCT allows for high axial resolution, which is limited in AO-SLO. Dual AO-OCT/AO-SLO systems record SLO and OCT images simultaneously with pixel-to-pixel correspondence. This technology can use the high axial resolution of AO-OCT to visualize different layers of the retina such as the inner and outer segments of the photoreceptor and the external limiting membrane (Dong et al. 2017, Felberer et al. 2014). The AO-SLO images can be used to facilitate image registration, correcting for eye movement artifacts and allowing cellular-level resolution of photoreceptors and retinal pigment epithelium. AO-OCT also permits the sensitivity and axial resolution that AO-SLO lacks in imaging the LC with depth, even though AO-SLO can provide very-high-resolution imaging of the LC surface (Vilupuru et al. 2007). Additionally, AO-OCT/AO-SLO systems can image retinal vessel walls and intravascular structures such as individual erythrocytes (Felberer et al. 2015). Another multimodal system is AO-OCT and AO–fundus camera imaging. AO–fundus camera imaging can be used to visualize photoreceptors (Lombardo et al. 2012), RNFL (Ramaswamy et al. 2014), and retinal capillaries (Popovic et al. 2011). AO–fundus camera imaging provides a large field of view, unlike limited AO-OCT and AO-SLO, although AO-OCT provides the depth information that enriches what is seen on AO–fundus camera images (Dong et al. 2017). Overall, AO-OCT has proven to be a promising and evolving technique that can play a valuable role in glaucoma evaluation. Currently, technological limitations, with regard to both field of view and image acquisition, hinder the clinical utility of AO-OCT and AO-SLO.

FUNCTIONAL OCT: DOPPLER OCT AND OCT-ANGIOGRAPHY

Although the pathogenesis of glaucoma is not fully understood, vascular dysfunction in the ONH may contribute to the development and progression of glaucoma (Cherecheanu et al. 2013, Flammer et al. 2002). Prior to the advent of OCT-angiography (OCTA), several technologies, including fluorescein angiography, indocyanine green angiography, laser Doppler flowmetry, and Doppler ultrasound, demonstrated impaired blood flow in retinal microvasculature but with their own limitations. Both fluorescein angiography and indocyanine green angiography are invasive modalities with potential side effects that have demonstrated alterations in blood flow in glaucoma qualitatively but are limited in resolution and ability to determine the exact locations of vascular dysfunction, especially with deeper ONH vasculature (Arend et al. 2004, Francois & de Laey 1974, Lee et al. 2017b, Werner & Shen 2019). Both laser Doppler flowmetry and laser speckle flowgraphy are noncontact methods that have shown lower blood flow in subjects with open-angle glaucoma than in healthy subjects but are limited owing to their measurement variability and restricted sampling area (Hafez et al. 2003, Nicolela et al. 1997, Piltz-Seymour 1999, Shiga et al. 2016). Color Doppler ultrasound is another noninvasive method that has shown reductions

in flow velocities and increased vascular resistance in glaucomatous eyes compared with healthy eyes. Color Doppler ultrasound requires a relatively long wavelength for sufficient penetration of deeper tissue and is therefore limited in resolution and its capacity to evaluate smaller retinal vessels (Chiou et al. 1999, Rankin 1999). Doppler OCT detects the Doppler frequency shift of back-scattered light to provide information about flow velocity and pulsatile flow dynamics (Leitgeb et al. 2003b, Wang et al. 2011, White et al. 2003). Like color Doppler ultrasound, Doppler OCT can determine total retinal blood flow and flow information in larger vessels; both of these methods lack the sensitivity to detect microcirculatory flow or areas of low flow velocity, especially given their reliance on the orientation of the vessel relative to the incident ultrasound or OCT beam (Chen & Wang 2017, Jia et al. 2012, Wang et al. 2011, Zhang et al. 2015). Magnetic resonance imaging has been used for quantifying ONH blood flow but is limited in its sensitivity for detecting microcirculatory blood flow and focal defects (Prünte et al. 1995).

OCTA is a useful noninvasive technique to assess ocular circulation in the ONH, peripapillary retina, and macula (C.L. Chen et al. 2016a,b; H.S. Chen et al. 2017; Jia et al. 2012, 2014; Kwon et al. 2017; Liu et al. 2015; Yarmohammadi et al. 2017). OCTA can depict vasculature with flowing blood by comparing reflectance signals between serial scans of the same tissue area over time. Areas of changing reflectance are shown as bright pixels and areas of static reflectance as dark pixels. Because reflectance signals of an area in the retina should be constant over serially acquired scans, moving objects, in particular, red blood cells dynamically flowing through vasculature, are detected by this technique. Therefore, OCTA uses blood flow as a type of intrinsic contrast agent and does not require the injection of a dye to map retinal vasculature. In addition, unlike dye-based angiography, OCTA is depth resolved and reveals multiple vascular plexes within different retinal layers. Other advantages include fast scanning speed, high image resolution, good interobserver and interscan reproducibility, and volumetric vascular data that can provide specific information about the location of vascular abnormalities (Chen & Wang 2017, Liu et al. 2015, Werner & Shen 2019).

Multiple change quantification methods are used for OCT reflectance signals: phase-signal-based, intensity-signal-based, and complex-signal-based techniques. Phase-signal-based techniques measure the variance of the phase shift of light in successive B-scans, which depends less on vessel orientation, whereas Doppler OCT uses the phase difference between scans (Chen & Wang 2017). Intensity-signal-based OCTA techniques enhance flow signals by comparing the amplitude (i.e., the intensity) of the reflectance signals between serial scans; a constant signal comes from static tissue and a variable signal comes from dynamic structures (i.e., blood). The complex-signal-based techniques combine both signal phase and intensity information to improve sensitivity to flow. OCTA provides quantitative metrics, such as vessel density (VD) and flow index (FI), that indirectly assess ocular blood flow (Figure 5). No studies to date have established how these metrics relate to true blood flow and VD (Chansangpetch & Lin 2018, Jia et al. 2014).

Overall, studies using these OCTA algorithms have found evidence of vascular compromise in glaucoma. Initial studies demonstrated significantly reduced FI and VD in the ONH and peripapillary retina in eyes with preperimetric and perimetric primary open-angle

glaucoma (POAG) compared with healthy eyes, with evidence of visualizable focal defects in glaucomatous eyes (Jia et al. 2012, 2014; Liu et al. 2015). Subsequent studies have further confirmed this finding and have shown that macular VDs also tend to be reduced in glaucomatous eyes compared to healthy eyes (Alnawaiseh et al. 2018, Chen & Wang 2017, Hou et al. 2018, Yarmohammadi et al. 2017). Other studies have since demonstrated the presence of peripapillary deep-layer microvasculature dropout, or the complete loss of the microvasculature within the β zone of peripapillary atrophy in patients with POAG (Lee et al. 2017a, Suh et al. 2016). OCTA parameters were also examined in different glaucoma subtypes. For example, VDs are reduced in normal-tension glaucoma, with no significant difference when compared with severity-matched POAG eyes (Bojikian et al. 2016, Scripsema et al. 2016). VDs are also reduced in eyes with pseudoexfoliative glaucoma, with greater reductions when compared with severity-matched POAG eyes (J.H. Park et al. 2018, Philip et al. 2019, Suwan et al. 2018). OCTA measurements were reduced in eyes with primary angle-closure glaucoma compared with control eyes (Rao et al. 2017e, S. Zhang et al. 2017).

The studies of VD in glaucomatous eyes suggest that VD reduction in glaucoma is a secondary rather than a primary effect. The loss of RGCs and their axons and dendrites follows a specific, characteristic pattern in glaucoma, that is, an arcuate loss of tissue extending and expanding from the ONH. This pattern speaks to glaucomatous injury at the LC. The pattern of reduction in VD is the same as that of neural tissue loss, yet there is no single point source to explain this. Rather, the VD reduction pattern suggests that the VD is diminished because there is less tissue to supply. This secondary role of VD demonstrated by OCTA may also help explain the closer association between VD and the visual field than between neural structural measures and functional assessment by visual field testing.

Many studies have examined how OCTA assessment of vascular function has correlated with existing measurements used in current glaucoma evaluation through visual field testing and conventional OCT. Studies have shown VD is significantly associated with the severity of functional loss in visual field testing, and even more so than circumpapillary RNFL and macular GCC thickness in some studies (Alnawaiseh et al. 2018; Holló 2017b; Jia et al. 2014; Jo et al. 2018; Liu et al. 2015; Penteado et al. 2018; Wang et al. 2015; Yarmohammadi et al. 2016, 2017). In addition to correlating with functional loss, OCTA vascular measurements also correlate well with structural damage, as indicated by RNFL and GCIPL thickness (Alnawaiseh et al. 2018, C.L. Chen et al. 2017, Pradhan et al. 2018, Wang et al. 2015). The extent of the correlation of VD and FI with structural damage and functional loss can vary by sector (Holló 2017b; Pradhan et al. 2018; Rao et al. 2017b, 2018; Sakaguchi et al. 2017). Notably, a subset of these investigations examined glaucomatous eyes with a single hemi-field defect, which have demonstrated reductions in VD and FI even in the perimetrically unaffected hemiretinae of these eyes. These studies still demonstrate significant correlations between OCTA parameters with structural OCT parameters and visual field parameters, but these associations appear to vary sectorally; Pradhan et al. (2018) found the temporal sector had reduced VD despite normal RNFL thickness (C.L. Chen et al. 2017, Yarmohammadi et al. 2017). This finding suggests that there is potential to identify change in OCTA-derived parameters in certain sectors before abnormalities in RNFL thickness are detected. A topographic association between the

location of deep-layer microvasculature dropout and the location of visual field damage and structural defects in the LC and RNFL has also been reported (Lee et al. 2017a; Shin et al. 2019; Suh et al. 2016, 2018). Additionally, studies have found a stronger correlation between visual field parameters and VD than between visual field parameters and RNFL thickness in glaucomatous eyes with high myopia but not in glaucomatous eyes without high myopia. Thus, there appears to be utility in OCTA for the assessment of highly myopic eyes for glaucoma, as highly myopic eyes can have nonglaucomatous RNFL thinning (Shin et al. 2019). Furthermore, OCTA-derived macular VD shows promise for monitoring late-stage progression especially beyond −14 dB, because unlike OCT measurements such as circumpapillary RNFL and GCC thickness, no measurement floor has been identified beyond which glaucomatous change is undetectable (Moghimi et al. 2019).

The diagnostic ability of OCTA measurements in relation to structural OCT parameters has been examined in prior investigations. Overall, the AUCs and sensitivities for distinguishing glaucomatous eyes from healthy eyes were roughly similar for OCTA-derived peripapillary and macular VD parameters and OCT-derived RNFL or GCC thickness, respectively; however, some studies have shown that RNFL or GCC thickness may be superior to VD parameters in discriminating ability, whereas other studies have shown the opposite (Chung et al. 2017; Hou et al. 2019; Kumar et al. 2016; Kurysheva et al. 2018; Penteado et al. 2018; Rao et al. 2017a,d; Triolo et al. 2017; Wan et al. 2018; Yarmohammadi et al. 2016). Given the relatively recent introduction of OCTA, short-term longitudinal studies have also demonstrated that OCTA can detect progressive glaucomatous change even without evidence of change in conventional structural parameters (Hou et al. 2019, Shoji et al. 2017). Lower baseline macular and ONH VDs were associated with faster rates of RNFL progression, speaking to the role of evaluating risk of glaucoma progression by OCTA (Moghimi et al. 2018). Studies have also demonstrated a significant correlation between the presence of parapapillary choroidal microvasculature dropout and longitudinal RNFL thinning (Lin et al. 2019, H.L. Park et al. 2018) and central visual field progression in patients with glaucoma (Jo et al. 2019, Kwon et al. 2019). Enlargement of this microvasculature dropout occurred with progressive longitudinal RNFL thinning in POAG (Kim et al. 2019).

OCTA has limitations. Shadowing artifacts, which are signal attenuations that occur when the OCT signal is blocked or absorbed; motion artifacts from patient movement in the setting of OCTA's relatively long acquisition times; and segmentation artifacts can occur. Projection artifacts are especially important to consider when interpreting OCTA images. This occurs when incident OCT light reaches superficial blood vessels and, instead of being reflected and captured by the detector, passes through blood to more reflective tissues deep to the vessels, where it back-scatters and produces ghost, or false, vascular networks on a deeper retinal layer (Borrelli et al. 2019, Chen & Wang 2017, Jia et al. 2012, Spaide et al. 2015). Many strategies, such as the incorporation of eye-tracking technologies to address motion artifacts, the use of projection-resolved algorithms to suppress projection artifacts, and the use of high-density scanning to improve scan resolution, have been developed to improve the quality of images that some studies have previously described as poor (Camino et al. 2016, Patel et al. 2018, Venugopal et al. 2019). Studies have shown that intravisit and intervisit reproducibility of OCTA VD measurements was better than that of average RNFL and GCC thickness, with some studies demonstrating worse intervisit reproducibility

of OCTA in glaucomatous eyes (Manalastas et al. 2017, Venugopal et al. 2018). Part of the source of the variability is the dependence of OCTA parameters on, for example, intraocular pressure, systemic perfusion, and medications, which should be considered when interpreting each scan (Alnawaiseh et al. 2018, Fuchsjäger-Mayrl et al. 2005, Holló 2017a, Mansouri et al. 2018, Rao et al. 2017c).

VISIBLE-LIGHT OCT

As mentioned above, conventional OCT systems use NIR light to produce 3D in vivo images. NIR light is well suited for ocular imaging because it is minimally absorbed and scattered in living tissue, allowing for greater depth of penetration. The availability of NIR broadband light sources, primarily related to their global use in telecommunications, has also contributed to its widespread adoption in OCT technology (S. Chen et al. 2016, Swanson & Fujimoto 2017). However, visible-light OCT (Vis-OCT) uses shorter wavelengths, enabling higher axial resolution with a similar spectral bandwidth, a stronger back-scattered signal given the inverse correlation of optical scattering in biological tissue with wavelength, and a higher lateral resolution (Bizheva et al. 2017, S. Chen et al. 2016, Jacques 2013, Povazay et al. 2002, Shu et al. 2017). Vis-OCT also offers an increase in optical absorption and scattering contrasts but compromises depth of penetration (Shu et al. 2019).

Applicability of Vis-OCT for glaucoma detection can be appreciated when examining the retinal layers. The optical properties of RNFL can provide information about changes occurring at the level of axonal structure even before detectable evidence of axonal degeneration and changes in RNFL thickness (Zhang et al. 2011). A rat model of glaucoma demonstrated that a change in optical reflectance of RNFL, which arises from scattering by cylindrical axonal ultrastructure, precedes apparent histological changes in the axonal cytoskeleton and RNFL thinning, suggesting RNFL optical properties can offer an early sign of glaucomatous damage (Huang & Knighton 2005, Huang et al. 2011b, Knighton & Huang 1999). Change in RNFL reflectance intensity can improve the predictive ability of the rate of RNFL thinning for a particular rate of functional deterioration (Gardiner et al. 2016). Studies have shown promise for the role of RNFL reflectance in early glaucoma diagnosis (Liu et al. 2014). At shorter wavelengths (~570 nm) the reflectance comes from cylinders with diameters much smaller relative to the wavelength, but with longer wavelengths (>680 nm) the reflectance from cylinders ranges from 350 to 900 nm (Knighton & Huang 1999). At shorter wavelengths the optical reflectance of damaged RNFL is less than that at longer wavelengths (Huang et al. 2011a, Zhang et al. 2011). Thus, OCT systems that incorporate the visible-light spectrum are more sensitive to the reflectance of thin cylindrical structures found in the RNFL and may be able to detect early glaucomatous change owing to increased spectral contrast at shorter wavelengths (Zhang et al. 2011). Additionally, the retinal IPL contains ganglion cell dendrites arranged into five layers, three inner “on” and two outer “off” sublaminae, and is where very early glaucomatous changes may occur. Histologic changes first occur in the outermost layer of the IPL, the “off” sublaminae of the IPL, in experimental animal models of glaucoma (El-Danaf & Huberman 2015, Ou et al. 2016). The in vivo visualization and assessment of the layers of the IPL, which can offer new imaging biomarkers for earlier glaucoma detection and monitoring, have been a challenge

with conventional OCT systems. Recent investigation introducing new advances into Vis-OCT technology demonstrates visualization of all five layers of the IPL, offering potential biomarkers in IPL sublamina thickness, reflectance, and interlayer contrast (Zhang et al. 2019).

Another major advantage of Vis-OCT is the capability to assess retinal oxygenation and metabolism. Ocular blood flow, although informative, is often used as a proxy for oxygen and nutrient delivery to tissues. Retinal oximetry, however, can directly provide information about retinal oxygen utilization, specifically within the context of its role in the pathogenesis and progression of glaucoma. Studies have specifically supported the role of hypoxia in glaucomatous retinal damage. Prior investigations, including experimental animal models of glaucoma, have found elevated levels of hypoxia-inducible factor-1α (HIF-1α), a transcription factor associated with hypoxic stress, in the ONH and retinas of glaucomatous eyes compared with healthy eyes (Ergorul et al. 2010, Tezel & Wax 2004). Retinal blood oxygen saturation rate (sO_2), which is the ratio of oxygenated hemoglobin to total hemoglobin in arteries and veins, could be an important physiological parameter for monitoring oxygen metabolism in glaucoma. Previously, oxygen electrodes and magnetic resonance imaging have been used to quantitatively map ocular oxygenation but were limited owing to their highly invasive nature and restricted spatial resolution (Berkowitz & Wilson 1995). Fundus photography (Beach et al. 1999) and SLO (Kristjansdottir et al. 2014) are two noninvasive methods that have been used to determine sO_2, but their 2D nature introduces significant error (Pi et al. 2018). Prior studies using fundus photography have shown that subjects with advanced POAG had higher sO_2 in venules and a decreased arteriovenous difference in sO_2 compared with healthy subjects, but found no difference in sO_2 when considering subjects with mild glaucoma or subjects with the full spectrum of glaucoma severity. The decrease in arteriovenous difference in advanced glaucoma is thought to be due to lower oxygen consumption by damaged tissue (Olafsdottir et al. 2011, 2014; Vandewalle et al. 2014). Photoacoustic ocular imaging, a 3D modality that uses a pulsed laser to induce a photoacoustic signal that is then detected by an ultrasonic transducer at the eyelid, can determine sO_2 and, when combined with SD-OCT, can quantify retinal oxygen metabolic rate ($rMRO_2$) by simultaneously measuring blood flow rate (Jiao et al. 2010; Liu et al. 2011; Song et al. 2013, 2014; Zhang et al. 2006). To date, technical limitations have prevented the use of photoacoustic retinal imaging in humans.

Vis-OCT is another 3D modality that has noteworthy applications in retinal oximetry comparable with those of NIR-OCT. Measurements of sO_2 are based on the different absorption of hemoglobin when it is in its oxyhemoglobin (HbO_2) form and deoxyhemoglobin (Hb) form. The visible range of light offers advantages over the NIR range of light: The two forms of hemoglobin much more strongly absorb light, water molecules only minimally absorb light, and there is excellent contrast between HbO_2 and Hb for spectroscopic analysis (Pi et al. 2018). Studies have measured sO_2 (Figure 6) and, when simultaneously measured with blood flow, metabolic parameters such as total retinal oxygen delivery, oxygen extraction fraction, and $rMRO_2$ (Shu et al. 2017; Yi et al. 2014, 2015). A visible-light and NIR dual-band system that was constructed with a single supercontinuum laser revealed that, compared with NIR-OCT imaging, Vis-OCT was better able to distinguish the retinal pigment epithelium–choroid complex owing to better axial

resolution; had more depth-dependent visible-light dissipation, leading to limited imaging beyond the RPE; and had higher RNFL contrast, comparable blood flow measurements, and superior sO_2 estimation (S. Chen et al. 2017).

Vis-OCT has several potential limitations. Because the retina is particularly sensitive to visible light, Vis-OCT image acquisition can cause subject discomfort and can distract gaze from the fixation target, inducing motion artifacts. Furthermore, visible light has higher phototoxicity at a given incident power; therefore, lower power must be used for imaging, reducing SNR. This results in imaging sensitivity with Vis-OCT that is lower than that with commercial NIR-OCTs. Additionally, transmission of visible light through the cornea and lens is attenuated relative to NIR light owing to high scattering, potentially affecting scan quality in the setting of aging or media opacification (Chong et al. 2017; Shu et al. 2017, 2019). Recent work has aimed to employ new strategies to improve performance and to optimize Vis-OCT technology for human retinal imaging over a broad range of eye diseases, which holds promise for further investigation of glaucoma and also utility in clinical glaucoma assessment (S. Chen et al. 2017, Shu et al. 2019).

ARTIFICIAL INTELLIGENCE

Artificial intelligence (AI) broadly refers to a field of computer science that involves the automation of tasks that traditionally require human intelligence. Machine learning (ML) is a subset of AI that uses data to build models called machine learning classifiers (MLCs), which generate predictions that grade or classify a particular input. Supervised ML methods rely on preexisting ground truths usually in the form of human-labeled training data to guide outputs. Unsupervised ML methods generate outputs from raw data without human guidance other than being programmed with mountains of data to then discriminate internally. This results in a black box interpretation by the computer algorithms, which find differentiating characteristics within datasets that may or may not be identifiable by conventional means. For example, in a 2018 study, a deep learning (DL) algorithm could discriminate subject gender from fundus photos—a task impossible for humans evaluating the same set of images (Poplin et al. 2018). Artificial neural networks (ANNs) are an ML method modeled after central nervous system processing that occur in the visual pathway at the level of neurons. ANN architecture involves nodes, theoretically functioning as neurons, which provide and receive information to and from other nodes. The nodes are arranged into a layer of data input, several intermediary layers, and a layer of data output. DL is a computationally intensive iteration of ANN that uses several intermediary layers of processing to learn and generate more accurate and complex outputs for increasingly complex inputs, such as raw images. Convolutional neural networks (CNNs), a subtype of DL, use filter functions to extract certain features from images (Figure 7). It is thus feature agnostic, not requiring determinations by humans to guide processing. Layers of weighted feature extraction and data representation are synthesized to produce the intended classification. Importance is applied to each node on the basis of an iterative training process that determines the optimal weights that yield the smallest classification error (LeCun et al. 2015, Zheng et al. 2019).

As the field of AI has expanded and shown great applicability in a wide range of fields in recent years, it has shown immense promise for glaucoma detection. Initially, extensive

work with ML using visual fields to distinguish normal from glaucomatous visual fields performed well compared with global indices of standard automated perimetry and experts (Asaoka et al. 2016, Chan et al. 2002, Goldbaum et al. 1994). AI has also been able to identify glaucomatous visual field progression (Goldbaum et al. 2012, Yousefi et al. 2018). ML has also been used with structural information from imaging to aid in glaucoma detection and management. AI classification techniques for the detection of glaucoma using SLO and scanning laser polarimetry have shown some success, but these methods have fallen out of favor in clinical use owing to advances in other ophthalmic imaging (Bowd et al. 2002, 2004, 2005; Lally et al. 2009; Zangwill et al. 2004). Image classification DL methods for the detection of referable glaucomatous optic neuropathy on fundus photos achieved AUCs as high as 0.98 with relatively high sensitivity and specificity when compared with clinical providers (Li et al. 2018, Phene et al. 2019, Ting et al. 2017). With the advent of OCT, the applicability of AI using OCT imaging has also been explored. The earliest studies that used TD-OCT parameters achieved AUCs as high as 0.991 with high sensitivities and specificities for detecting glaucomatous abnormalities (Burgansky-Eliash et al. 2005, Huang & Chen 2005). AI algorithms using SD-OCT parameters have demonstrated good diagnostic performance (Bizios et al. 2010, Grewal et al. 2008) but were not superior to the best-performing OCT parameters (Barella et al. 2013, Vidotti et al. 2013). The incorporation of OCTA-derived VD into neural networks also improves diagnostic performance of other OCT parameters such as GCIPL thickness (K. Park et al. 2018). ML methods combining functional and structural OCT parameters increase performance compared with methods using either parameter alone (Bowd et al. 2008, 2012; Kim et al. 2017).

As with diagnostic studies using fundus photos, DL methods have enabled the use of more complex inputs, such as those from OCT scans and probability maps generated from OCT scans. DL algorithms using SD-OCT and SS-OCT scans of the ONH and macula have achieved high diagnostic performance differentiating glaucoma-suspect eyes from glaucomatous and healthy eyes as well as detecting glaucoma progression; some studies have demonstrated performance superior to that of conventional global and sectoral OCT parameters as well as standard automated perimetry parameters (Asaoka et al. 2019; Christopher et al. 2018; Lee et al. 2020a,b; Muhammad et al. 2017). It is important to recognize that the performance of the employed algorithms is dependent on the quality of the OCT scans and on their segmentation, measurements, and maps if employed for analysis. Additionally, these algorithms may include or exclude valuable information from unconventional sources, such as from tissue reflectance or other raw imaging data, that has yet to be identified as useful.

In one approach, AI algorithms can improve OCT scan quality by using promising denoising efforts (Devalla et al. 2019, Gisbert et al. 2020, Halupka et al. 2018, Huang et al. 2019). One such study used AI for denoising on OCT B-scans of the ONH, which dramatically improved the quality of OCT scans while reducing scanning times and minimizing patient discomfort (Devalla et al. 2019). AI can also be used to enhance OCT segmentation, which has implications for glaucoma disease modeling, particularly at the ONH (Miri et al. 2015, 2017; Zheng et al. 2019). Some investigators effectively digitally stained neural and connective tissue layers of the ONH, including retinal layers, and the LC using DL, allowing

for automated structural measurements (Devalla et al. 2018). Maetschke et al. (2019b) used a feature-agnostic CNN approach to classify glaucomatous eyes with raw unsegmented 3D OCT volumes of the ONH rather than with parameters conventionally associated with glaucoma. They found that this was superior to measurements of RNFL thickness in the classification of glaucoma disease status. Class activation maps, a method used to visualize the data within an image area that a CNN uses in its classification (Zhou et al. 2016), provided insight into the regions of OCT volumes that were important for glaucoma detection. In addition to established clinical markers of glaucoma, including the neuroretinal rim and optic disc cupping, the LC and its surrounding regions were also consistently identified, which is in line with recent studies recognizing the LC as an important structure that can be visualized with OCT in glaucomatous eyes, offering new potential areas for glaucoma evaluation (Maetschke et al. 2019b). Another study by Maetschke et al. (2019a) demonstrated the use of a CNN on raw OCT data to estimate global visual field parameters, visual field index and mean deviation, in healthy patients and patients with glaucoma. CNN was superior to other ML methods using conventional features. Thompson et al. (2020) used a segmentation-free DL algorithm to diagnose glaucoma with performance superior to that of RNFL thickness parameters determined using conventional segmentation. DL using feature agnostic analysis of raw OCT data appears to be a promising, efficient, and cost-friendly alternative that may be superior to existing methods for identifying glaucoma and its progression.

Last, using anterior segment OCT, ML has proven to be useful in both the automated detection of angle closure and the identification of its mechanism (Fu et al. 2019; Niwas et al. 2016; Xu et al. 2013, 2019).

FUTURE OF OCT

In just a matter of a few decades since its inception, OCT has become a powerful, constantly evolving mainstay. Swanson & Fujimoto (2017) identified the following features of the surrounding ecosystem that were critical to the success of OCT: the physics principles that allow for impressive performance at a relatively low cost; government research funding; competition and collaboration fostered by the existing academic research infrastructure; interdisciplinary innovation; the ability to address real clinical needs that improve care and lower costs; entrepreneurism and large-scale investments; and the ongoing economic, scientific, and clinical impacts that reinforce and self-sustain the ecosystem for continued use and growth.

Intraoperative OCT (iOCT) is a potential application for the management of glaucoma that can add to and reinforce this ecosystem. iOCT was first introduced in the 1990s and has since emerged as an adjunct to ophthalmic surgery. Initially, the integration of SD-OCT into ophthalmic surgery involved portable OCT devices in the operating room that were handheld, externally mounted, or microscope-mounted, and required interruptions during the surgical procedure in order to acquire images. Advances in multimodal technology, such as the microscope-integrated iOCT system, have transformed surgery by providing the ability to visualize in real time structures that previously could not be seen, potentially impacting decision-making as the surgery is happening (Ehlers et al. 2014b). iOCT has been used

in both anterior segment and posterior segment surgeries, including glaucoma surgeries such as trabeculectomy and tube implants (Ang et al. 2020, Ehlers et al. 2014a). Some barriers to widespread clinical use in glaucoma surgery include cost; a steep learning curve; lag between real-time surgical movement and the image display; limited light penetration; motion artifact from eye movement; and obstruction, shadowing, and reflectivity by metal instruments and the sclera (Ang et al. 2020, Heindl et al. 2015, Junker et al. 2017). Future technological advances addressing these limitations, such as lag-free live OCT images, OCT-compatible surgical instruments, and SS-OCT, can potentially lead to integration into the routine surgical practice (Ang et al. 2020; Ehlers et al. 2014b, 2015).

Teleophthalmology, a branch of telemedicine that delivers care through the intersection of telecommunications and digital medical equipment, can also be impacted by the incorporation of OCT. Teleophthalmology is particularly suited for connecting clinicians to underserved and remote populations. For example, glaucoma is a disease that preferentially affects older adults. Glaucoma and other vision-impairing diseases can impact the quality of life of older adults through an increased risk of depression, decreased social engagement, and impaired activities of daily living and employment, all of which can ultimately impact access to health care (Jin et al. 2019, Umfress & Brantley 2016, Wang et al. 2012). Furthermore, populations of African descent have a significantly higher prevalence of POAG and higher rates of blindness. Studies have demonstrated notable differences in treatment rates for black populations compared with white populations, suggesting undertreatment as a reason for this disparity (Javitt et al. 1991). Regular and frequent clinical visits are required to detect glaucoma and monitor its progression, and clinical management should be individualized accordingly. Thus, while access to care may be increasingly limited in certain populations, the demands of preventing glaucoma from progressing continue to exist. Home monitoring offers a new way to expand care to nontraditional settings in order to facilitate effective care and improve patient outcomes. Self-tonometers for measuring intraocular pressure outside the office have been proposed in the past. One such device is a commercially available tonometer called iCare HOME (iCare Finland Oy; http://www.icarefinland.com/), which has shown reasonable feasibility and accuracy (Rojas et al. 2020, Takagi et al. 2017). Both Notal Vision (Manassas, Virginia; https://notalvision.com/) and Kubota Vision, Inc. (Seattle, Washington; https://www.kubotavision.com/) have developed preclinical home-based OCT devices that are reported to be lightweight, user friendly, and technician-free and are expected to be on the market soon. The Notal Vision unit is reportedly AI-based to allow automated identification of intra- or subretinal fluid in eyes with exudative age-related macular degeneration. Health care providers are able to use their cloud-based platform to monitor patients between regularly scheduled visits. Although it may be some time before the necessary quality for glaucoma monitoring is achieved, the potential translation to home monitoring glaucoma is not hard to imagine. Coupled with home perimetry (which is even closer than home-based OCT to becoming a clinical reality) and the potential role of AI, home health care delivery could have a large societal and economic impact by way of more accessible detection and prevention of irreversible glaucoma damage and related health care cost savings.

In summary, OCT technology has dramatically transformed the clinical management of glaucoma. With constantly evolving innovation and growing applicability, the future of OCT for glaucoma diagnosis and management remains bright.

ACKNOWLEDGMENTS

The authors acknowledge funding from the National Institutes of Health (grant R01-EY013178) and an unrestricted grant from Research to Prevent Blindness to the Department of Ophthalmology, NYU Langone Health, NYU Grossman School of Medicine.

LITERATURE CITED

Adhi M, Liu JJ, Qavi AH, Grulkowski I, Lu CD, et al. 2014. Choroidal analysis in healthy eyes using swept-source optical coherence tomography compared to spectral domain optical coherence tomography. Am. J. Ophthalmol 157:1272–81.e1 [PubMed: 24561169]

Alnawaiseh M, Lahme L, Müller V, Rosentreter A, Eter N. 2018. Correlation of flow density, as measured using optical coherence tomography angiography, with structural and functional parameters in glaucoma patients. Graefes Arch. Clin. Exp. Ophthalmol 256:589–97 [PubMed: 29332249]

Ang BCH, Lim SY, Dorairaj S. 2020. Intra-operative optical coherence tomography in glaucoma surgery—a systematic review. Eye 34:168–77 [PubMed: 31772380]

Arend O, Plange N, Sponsel WE, Remky A. 2004. Pathogenetic aspects of the glaucomatous optic neuropathy: fluorescein angiographic findings in patients with primary open angle glaucoma. Brain Res. Bull 62:517–24 [PubMed: 15036566]

Asaoka R, Murata H, Hirasawa K, Fujino Y, Matsuura M, et al. 2019. Using deep learning and transfer learning to accurately diagnose early-onset glaucoma from macular optical coherence tomography images. Am. J. Ophthalmol 198:136–45 [PubMed: 30316669]

Asaoka R, Murata H, Iwase A, Araie M. 2016. Detecting preperimetric glaucoma with standard automated perimetry using a deep learning classifier. Ophthalmology 123:1974–80 [PubMed: 27395766]

Barella KA, Costa VP, Gonçalves Vidotti V, Silva FR, Dias M, Gomi ES. 2013. Glaucoma diagnostic accuracy of machine learning classifiers using retinal nerve fiber layer and optic nerve data from SD-OCT. J. Ophthalmol 2013:789129 [PubMed: 24369495]

Beach JM, Schwenzer KJ, Srinivas S, Kim D, Tiedeman JS. 1999. Oximetry of retinal vessels by dual-wavelength imaging: calibration and influence of pigmentation. J. Appl. Physiol 86:748–58 [PubMed: 9931217]

Bengtsson B, Andersson S, Heijl A. 2012. Performance of time-domain and spectral-domain optical coherence tomography for glaucoma screening. Acta Ophthalmol 90:310–15 [PubMed: 20946342]

Berkowitz BA, Wilson CA. 1995. Quantitative mapping of ocular oxygenation using magnetic resonance imaging. Magn. Reson. Med 33:579–81 [PubMed: 7776892]

Biswas S, Lin C, Leung CKS. 2016. Evaluation of a myopic normative database for analysis of retinal nerve fiber layer thickness. JAMA Ophthalmol 134:1032–39 [PubMed: 27442185]

Bizheva K, Tan B, MacLelan B, Kralj O, Hajialamdari M, et al. 2017. Sub-micrometer axial resolution OCT for in-vivo imaging of the cellular structure of healthy and keratoconic human corneas. Biomed. Opt. Express 8:800–12 [PubMed: 28270986]

Bizios D, Heijl A, Hougaard JL, Bengtsson B. 2010. Machine learning classifiers for glaucoma diagnosis based on classification of retinal nerve fibre layer thickness parameters measured by Stratus OCT. Acta Ophthalmol 88:44–52 [PubMed: 20064122]

Bojikian KD, Chen CL, Wen JC, Zhang Q, Xin C, et al. 2016. Optic disc perfusion in primary open angle and normal tension glaucoma eyes using optical coherence tomography-based microangiography. PLOS ONE 11:e0154691 [PubMed: 27149261]

Borrelli E, Sadda SR, Uji A, Querques G. 2019. Pearls and pitfalls of optical coherence tomography angiography imaging: a review. Ophthalmol. Ther 8:215–26 [PubMed: 30868418]

Bowd C, Chan K, Zangwill LM, Goldbaum MH, Lee TW, et al. 2002. Comparing neural networks and linear discriminant functions for glaucoma detection using confocal scanning laser ophthalmoscopy of the optic disc. Investig. Ophthalmol. Vis. Sci 43:3444–54 [PubMed: 12407155]

Bowd C, Hao J, Tavares IM, Medeiros FA, Zangwill LM, et al. 2008. Bayesian machine learning classifiers for combining structural and functional measurements to classify healthy and glaucomatous eyes. Investig. Ophthalmol. Vis. Sci 49:945–53 [PubMed: 18326717]

Bowd C, Lee I, Goldbaum MH, Balasubramanian M, Medeiros FA, et al. 2012. Predicting glaucomatous progression in glaucoma suspect eyes using relevance vector machine classifiers for combined structural and functional measurements. Investig. Ophthalmol. Vis. Sci 53:2382–89 [PubMed: 22427577]

Bowd C, Medeiros FA, Zhang Z, Zangwill LM, Hao J, et al. 2005. Relevance vector machine and support vector machine classifier analysis of scanning laser polarimetry retinal nerve fiber layer measurements. Investig. Ophthalmol. Vis. Sci 46:1322–29 [PubMed: 15790898]

Bowd C, Zangwill LM, Medeiros FA, Hao J, Chan K, et al. 2004. Confocal scanning laser ophthalmoscopy classifiers and stereophotograph evaluation for prediction of visual field abnormalities in glaucoma-suspect eyes. Investig. Ophthalmol. Vis. Sci 45:2255–62 [PubMed: 15223803]

Burgansky-Eliash Z, Wollstein G, Chu T, Ramsey JD, Glymour C, et al. 2005. Optical coherence tomography machine learning classifiers for glaucoma detection: a preliminary study. Investig. Ophthalmol. Vis. Sci 46:4147–52 [PubMed: 16249492]

Bussel II, Wollstein G, Schuman JS. 2014. OCT for glaucoma diagnosis, screening and detection of glaucoma progression. Br. J. Ophthalmol 98(Suppl. 2):ii15–19 [PubMed: 24357497]

Camino A, Zhang M, Gao SS, Hwang TS, Sharma U, et al. 2016. Evaluation of artifact reduction in optical coherence tomography angiography with real-time tracking and motion correction technology. Biomed. Opt. Express 7:3905–15 [PubMed: 27867702]

Castejón-Móchon JF, López-Gil N, Benito A, Artal P. 2002. Ocular wave-front aberration statistics in a normal young population. Vis. Res 42:1611–17 [PubMed: 12079789]

Chan K, Lee TW, Sample PA, Goldbaum MH, Weinreb RN, Sejnowski TJ. 2002. Comparison of machine learning and traditional classifiers in glaucoma diagnosis. IEEE Trans. Biomed. Eng 49:963–74 [PubMed: 12214886]

Chang RT, Singh K. 2013. Myopia and glaucoma: diagnostic and therapeutic challenges. Curr. Opin. Ophthalmol 24:96–101 [PubMed: 23542349]

Chansangpetch S, Lin SC. 2018. Optical coherence tomography angiography in glaucoma care. Curr. Eye Res 43:1067–82 [PubMed: 29757019]

Charman WN, Chateau N. 2003. The prospects for super-acuity: limits to visual performance after correction of monochromatic ocular aberration. Ophthalmic Physiol. Opt 23:479–93 [PubMed: 14622350]

Chen CL, Bojikian KD, Gupta D, Wen JC, Zhang Q, et al. 2016a. Optic nerve head perfusion in normal eyes and eyes with glaucoma using optical coherence tomography-based microangiography. Quant. Imaging Med. Surg 6:125–33 [PubMed: 27190764]

Chen CL, Bojikian KD, Wen JC, Zhang Q, Xin C, et al. 2017. Peripapillary retinal nerve fiber layer vascular microcirculation in eyes with glaucoma and single-hemifield visual field loss. JAMA Ophthalmol 135:461–68 [PubMed: 28358939]

Chen CL, Wang RK. 2017. Optical coherence tomography based angiography [Invited]. Biomed. Opt. Express 8:1056–82 [PubMed: 28271003]

Chen CL, Zhang A, Bojikian KD, Wen JC, Zhang Q, et al. 2016b. Peripapillary retinal nerve fiber layer vascular microcirculation in glaucoma using optical coherence tomography-based microangiography. Investig. Ophthalmol. Vis. Sci 57:OCT475–85 [PubMed: 27442341]

Chen HS, Liu CH, Wu WC, Tseng HJ, Lee YS. 2017. Optical coherence tomography angiography of the superficial microvasculature in the macular and peripapillary areas in glaucomatous and healthy eyes. Investig. Ophthalmol. Vis. Sci 58:3637–45 [PubMed: 28728171]

Chen S, Shu X, Nesper PL, Liu W, Fawzi AA, Zhang HF. 2017. Retinal oximetry in humans using visible-light optical coherence tomography [Invited]. Biomed. Opt. Express 8:1415–29 [PubMed: 28663838]

Chen S, Shu X, Yi J, Fawzi A, Zhang HF. 2016. Dual-band optical coherence tomography using a single supercontinuum laser source. J. Biomed. Opt 21:66013 [PubMed: 27304421]

Cherecheanu AP, Garhofer G, Schmidl D, Werkmeister R, Schmetterer L. 2013. Ocular perfusion pressure and ocular blood flow in glaucoma. Curr. Opin. Pharmacol 13:36–42 [PubMed: 23009741]

Chiou HJ, Chou YH, Liu CJ, Hsu CC, Tiu CM, et al. 1999. Evaluation of ocular arterial changes in glaucoma with color Doppler ultrasonography. J. Ultrasound Med 18:295–302 [PubMed: 10206218]

Cho JW, Sung KR, Hong JT, Um TW, Kang SY, Kook MS. 2011. Detection of glaucoma by spectral domain-scanning laser ophthalmoscopy/optical coherence tomography (SD-SLO/OCT) and time domain optical coherence tomography. J. Glaucoma 20:15–20 [PubMed: 20436370]

Choi SS, Zawadzki RJ, Lim MC, Brandt JD, Keltner JL, et al. 2011. Evidence of outer retinal changes in glaucoma patients as revealed by ultrahigh-resolution in vivo retinal imaging. Br. J. Ophthalmol 95:131–41 [PubMed: 20956277]

Choma M, Sarunic M, Yang C, Izatt J. 2003. Sensitivity advantage of swept source and Fourier domain optical coherence tomography. Opt. Express 11:2183–89 [PubMed: 19466106]

Chong SP, Bernucci M, Radhakrishnan H, Srinivasan VJ. 2017. Structural and functional human retinal imaging with a fiber-based visible light OCT ophthalmoscope. Biomed. Opt. Express 8:323–37 [PubMed: 28101421]

Christopher M, Belghith A, Weinreb RN, Bowd C, Goldbaum MH, et al. 2018. Retinal nerve fiber layer features identified by unsupervised machine learning on optical coherence tomography scans predict glaucoma progression. Investig. Ophthalmol. Vis. Sci 59:2748–56 [PubMed: 29860461]

Chung JK, Hwang YH, Wi JM, Kim M, Jung JJ. 2017. Glaucoma diagnostic ability of the optical coherence tomography angiography vessel density parameters. Curr. Eye Res 42:1458–67 [PubMed: 28910159]

Curcio CA, Allen KA. 1990. Topography of ganglion cells in human retina. J. Comp. Neurol 300:5–25 [PubMed: 2229487]

de Boer JF, Cense B, Park BH, Pierce MC, Tearney GJ, Bouma BE. 2003. Improved signal-to-noise ratio in spectral-domain compared with time-domain optical coherence tomography. Opt. Lett 28:2067–69 [PubMed: 14587817]

Devalla SK, Chin KS, Mari JM, Tun TA, Strouthidis NG, et al. 2018. A deep learning approach to digitally stain optical coherence tomography images of the optic nerve head. Investig. Ophthalmol. Vis. Sci 59:63–74 [PubMed: 29313052]

Devalla SK, Subramanian G, Pham TH, Wang X, Perera S, et al. 2019. A deep learning approach to denoise optical coherence tomography images of the optic nerve head. Sci. Rep 9:14454 [PubMed: 31595006]

Diaz-Santana L, Torti C, Munro I, Gasson P, Dainty C. 2003. Benefit of higher closed-loop bandwidths in ocular adaptive optics. Opt. Express 11:2597–605 [PubMed: 19471373]

Dong ZM, Wollstein G, Schuman JS. 2016. Clinical utility of optical coherence tomography in glaucoma. Investig. Ophthalmol. Vis. Sci 57:OCT556–67 [PubMed: 27537415]

Dong ZM, Wollstein G, Wang B, Schuman JS. 2017. Adaptive optics optical coherence tomography in glaucoma. Prog. Retin. Eye Res 57:76–88 [PubMed: 27916682]

Ehlers JP, Dupps WJ, Kaiser PK, Goshe J, Singh RP, et al. 2014a. The Prospective Intraoperative and Perioperative Ophthalmic ImagiNg with Optical CoherEncE TomogRaphy (PIONEER) study: 2-year results. Am. J. Ophthalmol 158:999–1007 [PubMed: 25077834]

Ehlers JP, Goshe J, Dupps WJ, Kaiser PK, Singh RP, et al. 2015. Determination of feasibility and utility of microscope-integrated optical coherence tomography during ophthalmic surgery: the DISCOVER Study RESCAN Results. JAMA Ophthalmol 133:1124–32 [PubMed: 26226623]

Ehlers JP, Srivastava SK, Feiler D, Noonan AI, Rollins AM, Tao YK. 2014b. Integrative advances for OCT-guided ophthalmic surgery and intraoperative OCT: microscope integration, surgical

instrumentation, and heads-up display surgeon feedback. PLOS ONE 9:e105224 [PubMed: 25141340]

El-Danaf RN, Huberman AD. 2015. Characteristic patterns of dendritic remodeling in early-stage glaucoma: evidence from genetically identified retinal ganglion cell types. J. Neurosci 35:2329–43 [PubMed: 25673829]

Ergorul C, Ray A, Huang W, Wang DY, Ben Y, et al. 2010. Hypoxia inducible factor-1α (HIF-1α) and some HIF-1 target genes are elevated in experimental glaucoma. J. Mol. Neurosci 42:183–91 [PubMed: 20237864]

Felberer F, Kroisamer JS, Baumann B, Zotter S, Schmidt-Erfurth U, et al. 2014. Adaptive optics SLO/OCT for 3D imaging of human photoreceptors in vivo. Biomed. Opt. Express 5:439–56 [PubMed: 24575339]

Felberer F, Rechenmacher M, Haindl R, Baumann B, Hitzenberger CK, Pircher M. 2015. Imaging of retinal vasculature using adaptive optics SLO/OCT. Biomed. Opt. Express 6:1407–18 [PubMed: 25909024]

Flammer J, Orgul S, Costa VP, Orzalesi N, Krieglstein GK, et al. 2002. The impact of ocular blood flow in glaucoma. Prog. Retin. Eye Res 21:359–93 [PubMed: 12150988]

Francois J, de Laey JJ. 1974. Fluorescein angiography of the glaucomatous disc. Ophthalmologica 168:288–98 [PubMed: 4209649]

Fu H, Baskaran M, Xu Y, Lin S, Wong DWK, et al. 2019. A deep learning system for automated angle-closure detection in anterior segment optical coherence tomography images. Am. J. Ophthalmol 203:37–45 [PubMed: 30849350]

Fuchsjäger-Mayrl G, Wally B, Rainer G, Buehl W, Aggermann T, et al. 2005. Effect of dorzolamide and timolol on ocular blood flow in patients with primary open angle glaucoma and ocular hypertension. Br. J. Ophthalmol 89:1293–97 [PubMed: 16170119]

Gardiner SK, Demirel S, Reynaud J, Fortune B. 2016. Changes in retinal nerve fiber layer reflectance intensity as a predictor of functional progression in glaucoma. Investig. Ophthalmol. Vis. Sci 57:1221–27 [PubMed: 26978028]

Ghasia FF, El-Dairi M, Freedman SF, Rajani A, Asrani S. 2015. Reproducibility of spectral-domain optical coherence tomography measurements in adult and pediatric glaucoma. J. Glaucoma 24:55–63 [PubMed: 23722865]

Girard MJ, Strouthidis NG, Ethier CR, Mari JM. 2011. Shadow removal and contrast enhancement in optical coherence tomography images of the human optic nerve head. Investig. Ophthalmol. Vis. Sci 52:7738–48 [PubMed: 21551412]

Gisbert G, Dey N, Ishikawa H, Schuman J, Fishbaugh J, Gerig G. 2020. Improved denoising of optical coherence tomography via repeated acquisitions and unsupervised deep learning. Investig. Ophthalmol. Vis. Sci 61:PB0035

Godara P, Dubis AM, Roorda A, Duncan JL, Carroll J. 2010. Adaptive optics retinal imaging: emerging clinical applications. Optom. Vis. Sci 87:930–41 [PubMed: 21057346]

Goldbaum MH, Lee I, Jang G, Balasubramanian M, Sample PA, et al. 2012. Progression of patterns (POP): a machine classifier algorithm to identify glaucoma progression in visual fields. Investig. Ophthalmol. Vis. Sci 53:6557–67 [PubMed: 22786913]

Goldbaum MH, Sample PA, White H, Côlt B, Raphaelian P, et al. 1994. Interpretation of automated perimetry for glaucoma by neural network. Investig. Ophthalmol. Vis. Sci 35:3362–73 [PubMed: 8056511]

Greenfield DS, Bagga H, Knighton RW. 2003. Macular thickness changes in glaucomatous optic neuropathy detected using optical coherence tomography. Arch. Ophthalmol 121:41–46 [PubMed: 12523883]

Grewal DS, Jain R, Grewal SP, Rihani V. 2008. Artificial neural network-based glaucoma diagnosis using retinal nerve fiber layer analysis. Eur. J. Ophthalmol 18:915–21 [PubMed: 18988162]

Grewal DS, Tanna AP. 2013. Diagnosis of glaucoma and detection of glaucoma progression using spectral domain optical coherence tomography. Curr. Opin. Ophthalmol 24:150–61 [PubMed: 23328662]

Guedes V, Schuman JS, Hertzmark E, Wollstein G, Correnti A, et al. 2003. Optical coherence tomography measurement of macular and nerve fiber layer thickness in normal and glaucomatous human eyes. Ophthalmology 110:177–89 [PubMed: 12511364]

Guirao A, Porter J, Williams DR, Cox IG. 2002. Calculated impact of higher-order monochromatic aberrations on retinal image quality in a population of human eyes. J. Opt. Soc. Am. A Opt. Image Sci. Vis 19:620–28 [PubMed: 11876329]

Hafez AS, Bizzarro RL, Lesk MR. 2003. Evaluation of optic nerve head and peripapillary retinal blood flow in glaucoma patients, ocular hypertensives, and normal subjects. Am. J. Ophthalmol 136:1022–31 [PubMed: 14644212]

Halupka KJ, Antony BJ, Lee MH, Lucy KA, Rai RS, et al. 2018. Retinal optical coherence tomography image enhancement via deep learning. Biomed. Opt. Express 9:6205–21 [PubMed: 31065423]

Hardin JS, Taibbi G, Nelson SC, Chao D, Vizzeri G. 2015. Factors affecting Cirrus-HD OCT optic disc scan quality: a review with case examples. J. Ophthalmol 2015:746150 [PubMed: 26351574]

Hee MR, Izatt JA, Swanson EA, Huang D, Schuman JS, et al. 1995. Optical coherence tomography of the human retina. Arch. Ophthalmol 113:325–32 [PubMed: 7887846]

Heindl LM, Siebelmann S, Dietlein T, Huttmann G, Lankenau E, et al. 2015. Future prospects: assessment of intraoperative optical coherence tomography in ab interno glaucoma surgery. Curr. Eye Res 40:1288–91 [PubMed: 25549053]

Hermann B, Fernández EJ, Unterhuber A, Sattmann H, Fercher AF, et al. 2004. Adaptive-optics ultrahigh-resolution optical coherence tomography. Opt. Lett 29:2142–44 [PubMed: 15460883]

Hofer H, Artal P, Singer B, Aragon JL, Williams DR. 2001. Dynamics of the eye's wave aberration. J. Opt. Soc. Am. A Opt. Image Sci. Vis 18:497–506 [PubMed: 11265680]

Holló G 2017a. Influence of large intraocular pressure reduction on peripapillary OCT vessel density in ocular hypertensive and glaucoma eyes. J. Glaucoma 26:e7–10 [PubMed: 27571444]

Holló G 2017b. Relationship between optical coherence tomography sector peripapillary angioflow-density and Octopus visual field cluster mean defect values. PLOS ONE 12:e0171541 [PubMed: 28152106]

Hou H, Moghimi S, Zangwill LM, Shoji T, Ghahari E, et al. 2018. Inter-eye asymmetry of optical coherence tomography angiography vessel density in bilateral glaucoma, glaucoma suspect, and healthy eyes. Am. J. Ophthalmol 190:69–77 [PubMed: 29580976]

Hou H, Moghimi S, Zangwill LM, Shoji T, Ghahari E, et al. 2019. Macula vessel density and thickness in early primary open-angle glaucoma. Am. J. Ophthalmol 199:120–32 [PubMed: 30496723]

Huang D, Swanson EA, Lin CP, Schuman JS, Stinson WG, et al. 1991. Optical coherence tomography. Science 254:1178–81 [PubMed: 1957169]

Huang ML, Chen HY. 2005. Development and comparison of automated classifiers for glaucoma diagnosis using Stratus optical coherence tomography. Investig. Ophthalmol. Vis. Sci 46:4121–29 [PubMed: 16249489]

Huang X-R, Knighton RW. 2005. Microtubules contribute to the birefringence of the retinal nerve fiber layer. Investig. Ophthalmol. Vis. Sci 46:4588–93 [PubMed: 16303953]

Huang X-R, Zhou Y, Kong W, Knighton RW. 2011a. Change of retinal nerve fiber layer reflectance correlated with cytostructural change in glaucoma. Investig. Ophthalmol. Vis. Sci 52:2442–42

Huang X-R, Zhou Y, Kong W, Knighton RW. 2011b. Reflectance decreases before thickness changes in the retinal nerve fiber layer in glaucomatous retinas. Investig. Ophthalmol. Vis. Sci 52:6737–42 [PubMed: 21730345]

Huang Y, Lu Z, Shao Z, Ran M, Zhou J, et al. 2019. Simultaneous denoising and super-resolution of optical coherence tomography images based on generative adversarial network. Opt. Express 27:12289–307 [PubMed: 31052772]

Huber R, Adler DC, Fujimoto JG. 2006a. Buffered Fourier domain mode locking: unidirectional swept laser sources for optical coherence tomography imaging at 370,000 lines/s. Opt. Lett 31:2975–77 [PubMed: 17001371]

Huber R, Adler DC, Srinivasan VJ, Fujimoto JG. 2007. Fourier domain mode locking at 1050 nm for ultra-high-speed optical coherence tomography of the human retina at 236,000 axial scans per second. Opt. Lett 32:2049–51 [PubMed: 17632639]

Huber R, Wojtkowski M, Fujimoto JG. 2006b. Fourier domain mode locking (FDML): a new laser operating regime and applications for optical coherence tomography. Opt. Express 14:3225–37 [PubMed: 19516464]

Jacques SL. 2013. Optical properties of biological tissues: a review. Phys. Med. Biol 58:R37–61 [PubMed: 23666068]

Javitt JC, McBean AM, Nicholson GA, Babish JD, Warren JL, Krakauer H. 1991. Undertreatment of glaucoma among black Americans. N. Engl. J. Med 325:1418–22 [PubMed: 1922253]

Jeoung JW, Choi YJ, Park KH, Kim DM. 2013. Macular ganglion cell imaging study: glaucoma diagnostic accuracy of spectral-domain optical coherence tomography. Investig. Ophthalmol. Vis. Sci 54:4422–29 [PubMed: 23722389]

Jeoung JW, Park KH. 2010. Comparison of Cirrus OCT and Stratus OCT on the ability to detect localized retinal nerve fiber layer defects in preperimetric glaucoma. Investig. Ophthalmol. Vis. Sci 51:938–45 [PubMed: 19797208]

Jia Y, Morrison JC, Tokayer J, Tan O, Lombardi L, et al. 2012. Quantitative OCT angiography of optic nerve head blood flow. Biomed. Opt. Express 3:3127–37 [PubMed: 23243564]

Jia Y, Wei E, Wang X, Zhang X, Morrison JC, et al. 2014. Optical coherence tomography angiography of optic disc perfusion in glaucoma. Ophthalmology 121:1322–32 [PubMed: 24629312]

Jian Y, Lee S, Ju MJ, Heisler M, Ding W, et al. 2016. Lens-based wavefront sensorless adaptive optics swept source OCT. Sci. Rep 6:27620 [PubMed: 27278853]

Jiao S, Jiang M, Hu J, Fawzi A, Zhou Q, et al. 2010. Photoacoustic ophthalmoscopy for in vivo retinal imaging. Opt. Express 18:3967–72 [PubMed: 20389409]

Jin S, Trope GE, Buys YM, Badley EM, Thavorn K, et al. 2019. Reduced social participation among seniors with self-reported visual impairment and glaucoma. PLOS ONE 14:e0218540 [PubMed: 31335896]

Jo YH, Kwon J, Jeong D, Shon K, Kook MS. 2019. Rapid central visual field progression rate in eyes with open-angle glaucoma and choroidal microvasculature dropout. Sci. Rep 9:8525 [PubMed: 31189960]

Jo YH, Sung KR, Yun SC. 2018. The relationship between peripapillary vascular density and visual field sensitivity in primary open-angle and angle-closure glaucoma. Investig. Ophthalmol. Vis. Sci 59:5862–67 [PubMed: 30550617]

Junker B, Jordan JF, Framme C, Pielen A. 2017. Intraoperative optical coherence tomography and ab interno trabecular meshwork surgery with the Trabectome. Clin. Ophthalmol 11:1755–60 [PubMed: 29026286]

Kapetanakis VV, Chan MP, Foster PJ, Cook DG, Owen CG, Rudnicka AR. 2016. Global variations and time trends in the prevalence of primary open angle glaucoma (POAG): a systematic review and meta-analysis. Br. J. Ophthalmol 100:86–93 [PubMed: 26286821]

Kim J-A, Lee EJ, Kim T-W. 2019. Evaluation of parapapillary choroidal microvasculature dropout and progressive retinal nerve fiber layer thinning in patients with glaucoma. JAMA Ophthalmol 137:810–16 [PubMed: 31120486]

Kim SJ, Cho KJ, Oh S. 2017. Development of machine learning models for diagnosis of glaucoma. PLOS ONE 12:e0177726 [PubMed: 28542342]

Kiumehr S, Park SC, Syril D, Teng CC, Tello C, et al. 2012. In vivo evaluation of focal lamina cribrosa defects in glaucoma. Arch. Ophthalmol 130:552–59 [PubMed: 22232364]

Knighton RW, Huang XR. 1999. Directional and spectral reflectance of the rat retinal nerve fiber layer. Investig. Ophthalmol. Vis. Sci 40:639–47 [PubMed: 10067967]

Kocaoglu OP, Cense B, Jonnal RS, Wang Q, Lee S, et al. 2011. Imaging retinal nerve fiber bundles using optical coherence tomography with adaptive optics. Vis. Res 51:1835–44 [PubMed: 21722662]

Kocaoglu OP, Turner TL, Liu Z, Miller DT. 2014. Adaptive optics optical coherence tomography at 1 MHz. Biomed. Opt. Express 5:4186–200 [PubMed: 25574431]

Kostanyan T, Wollstein G, Schuman JS. 2015. Evaluating glaucoma damage: emerging imaging technologies. Expert Rev. Ophthalmol 10:183–95 [PubMed: 27087829]

Kotowski J, Folio LS, Wollstein G, Ishikawa H, Ling Y, et al. 2012. Glaucoma discrimination of segmented Cirrus spectral domain optical coherence tomography (SD-OCT) macular scans. Br. J. Ophthalmol 96:1420–25 [PubMed: 22914498]

Kristjansdottir JV, Hardarson SH, Halldorsson GH, Karlsson RA, Eliasdottir TS, Stefánsson E. 2014. Retinal oximetry with a scanning laser ophthalmoscope. Investig. Ophthalmol. Vis. Sci 55:3120–26 [PubMed: 24736055]

Kumar RS, Anegondi N, Chandapura RS, Sudhakaran S, Kadambi SV, et al. 2016. Discriminant function of optical coherence tomography angiography to determine disease severity in glaucoma. Investig. Ophthalmol. Vis. Sci 57:6079–88 [PubMed: 27820876]

Kurysheva NI, Maslova EV, Zolnikova IV, Fomin AV, Lagutin MB. 2018. A comparative study of structural, functional and circulatory parameters in glaucoma diagnostics. PLOS ONE 13:e0201599 [PubMed: 30138396]

Kwon J, Choi J, Shin JW, Lee J, Kook MS. 2017. Alterations of the foveal avascular zone measured by optical coherence tomography angiography in glaucoma patients with central visual field defects. Investig. Ophthalmol. Vis. Sci 58:1637–45 [PubMed: 28297029]

Kwon JM, Weinreb RN, Zangwill LM, Suh MH. 2019. Parapapillary deep-layer microvasculature dropout and visual field progression in glaucoma. Am. J. Ophthalmol 200:65–75 [PubMed: 30578786]

Lally DR, Wollstein G, Danks D, Ishikawa H, Kagemann L, et al. 2009. Combining OCT, HRT, and GDx through machine learning classifiers for glaucoma detection. Investig. Ophthalmol. Vis. Sci 50:5817

LeCun Y, Bengio Y, Hinton G. 2015. Deep learning. Nature 521:436–44 [PubMed: 26017442]

Lee EJ, Kim T-W, Kim J-A, Kim J-A. 2017a. Parapapillary deep-layer microvasculature dropout in primary open-angle glaucoma eyes with a parapapillary γ-zone. Investig. Ophthalmol. Vis. Sci 58:5673–80 [PubMed: 29101405]

Lee EJ, Kim T-W, Weinreb RN, Park KH, Kim SH, Kim DM. 2011. Visualization of the lamina cribrosa using enhanced depth imaging spectral-domain optical coherence tomography. Am. J. Ophthalmol 152:87–95.e1 [PubMed: 21570046]

Lee EJ, Lee KM, Lee SH, Kim T-W. 2017b. Parapapillary choroidal microvasculature dropout in glaucoma: a comparison between optical coherence tomography angiography and indocyanine green angiography. Ophthalmology 124:1209–17 [PubMed: 28433445]

Lee J, Kim J-S, Lee HJ, Kim S-J, Kim YK, et al. 2020a. Discriminating glaucomatous and compressive optic neuropathy on spectral-domain optical coherence tomography with deep learning classifier. Br. J. Ophthalmol 104:1717–23 [PubMed: 32098860]

Lee J, Kim YK, Park KH, Jeoung JW. 2020b. Diagnosing glaucoma with spectral-domain optical coherence tomography using deep learning classifier. J. Glaucoma 29:287–94 [PubMed: 32053552]

Leitgeb R, Hitzenberger C, Fercher A. 2003a. Performance of Fourier domain versus time domain optical coherence tomography. Opt. Express 11:889–94 [PubMed: 19461802]

Leitgeb R, Schmetterer L, Drexler W, Fercher A, Zawadzki R, Bajraszewski T. 2003b. Real-time assessment of retinal blood flow with ultrafast acquisition by color Doppler Fourier domain optical coherence tomography. Opt. Express 11:3116–21 [PubMed: 19471434]

Leung CKS, Chan W-M, Yung W-H, Ng AC, Woo J, et al. 2005. Comparison of macular and peripapillary measurements for the detection of glaucoma: an optical coherence tomography study. Ophthalmology 112:391–400 [PubMed: 15745764]

Leung CKS, Ye C, Weinreb RN, Yu M, Lai G, Lam DS. 2013. Impact of age-related change of retinal nerve fiber layer and macular thicknesses on evaluation of glaucoma progression. Ophthalmology 120:2485–92 [PubMed: 23993360]

Leung CKS, Yu M, Weinreb RN, Ye C, Liu S, et al. 2012. Retinal nerve fiber layer imaging with spectral-domain optical coherence tomography: a prospective analysis of age-related loss. Ophthalmology 119:731–37 [PubMed: 22264886]

Li Z, He Y, Keel S, Meng W, Chang RT, He M. 2018. Efficacy of a deep learning system for detecting glaucomatous optic neuropathy based on color fundus photographs. Ophthalmology 125:1199–206 [PubMed: 29506863]

Lin S, Cheng H, Zhang S, Ye C, Pan X, et al. 2019. Parapapillary choroidal microvasculature dropout is associated with the decrease in retinal nerve fiber layer thickness: a prospective study. Investig. Ophthalmol. Vis. Sci 60:838–42 [PubMed: 30811547]

Lisboa R, Paranhos A Jr., Weinreb RN, Zangwill LM, Leite MT, Medeiros FA. 2013. Comparison of different spectral domain oct scanning protocols for diagnosing preperimetric glaucoma. Investig. Ophthalmol. Vis. Sci 54:3417–25 [PubMed: 23532529]

Liu L, Jia Y, Takusagawa HL, Pechauer AD, Edmunds B, et al. 2015. Optical coherence tomography angiography of the peripapillary retina in glaucoma. JAMA Ophthalmol 133:1045–52 [PubMed: 26203793]

Liu S, Wang B, Yin B, Milner TE, Markey MK, et al. 2014. Retinal nerve fiber layer reflectance for early glaucoma diagnosis. J. Glaucoma 23:e45–52 [PubMed: 23835671]

Liu T, Wei Q, Wang J, Jiao S, Zhang HF. 2011. Combined photoacoustic microscopy and optical coherence tomography can measure metabolic rate of oxygen. Biomed. Opt. Express 2:1359–65 [PubMed: 21559147]

Lombardo M, Serrao S, Devaney N, Parravano M, Lombardo G. 2012. Adaptive optics technology for high-resolution retinal imaging. Sensors 13:334–66 [PubMed: 23271600]

Maetschke S, Antony B, Ishikawa H, Wollstein G, Schuman J, Garnavi R. 2019a. Inference of visual field test performance from OCT volumes using deep learning. arXiv:1908.01428 [cs.CV]

Maetschke S, Antony B, Ishikawa H, Wollstein G, Schuman J, Garnavi R. 2019b. A feature agnostic approach for glaucoma detection in OCT volumes. PLOS ONE 14:e0219126 [PubMed: 31260494]

Manalastas PIC, Zangwill LM, Saunders LJ, Mansouri K, Belghith A, et al. 2017. Reproducibility of optical coherence tomography angiography macular and optic nerve head vascular density in glaucoma and healthy eyes. J. Glaucoma 26:851–59 [PubMed: 28858159]

Mansouri K, Rao HL, Hoskens K, D'Alessandro E, Flores-Reyes EM, et al. 2018. Diurnal variations of peripapillary and macular vessel density in glaucomatous eyes using optical coherence tomography angiography. J. Glaucoma 27:336–41 [PubMed: 29462016]

Mari JM, Strouthidis NG, Park SC, Girard MJ. 2013. Enhancement of lamina cribrosa visibility in optical coherence tomography images using adaptive compensation. Investig. Ophthalmol. Vis. Sci 54:2238–47 [PubMed: 23449723]

Miri MS, Abramoff MD, Kwon YH, Sonka M, Garvin MK. 2017. A machine-learning graph-based approach for 3D segmentation of Bruch's membrane opening from glaucomatous SD-OCT volumes. Med. Image Anal 39:206–17 [PubMed: 28528295]

Miri MS, Abramoff MD, Lee K, Niemeijer M, Wang JK, et al. 2015. Multimodal segmentation of optic disc and cup from SD-OCT and color fundus photographs using a machine-learning graph-based approach. IEEE Trans. Med. Imaging 34:1854–66 [PubMed: 25781623]

Moghimi S, Bowd C, Zangwill LM, Penteado RC, Hasenstab K, et al. 2019. Measurement floors and dynamic ranges of OCT and OCT angiography in glaucoma. Ophthalmology 126:980–88 [PubMed: 30858023]

Moghimi S, Zangwill LM, Penteado RC, Hasenstab K, Ghahari E, et al. 2018. Macular and optic nerve head vessel density and progressive retinal nerve fiber layer loss in glaucoma. Ophthalmology 125:1720–28 [PubMed: 29907322]

Mrejen S, Spaide RF. 2013. Optical coherence tomography: imaging of the choroid and beyond. Surv. Ophthalmol 58:387–429 [PubMed: 23916620]

Muhammad H, Fuchs TJ, De Cuir N, De Moraes CG, Blumberg DM, et al. 2017. Hybrid deep learning on single wide-field optical coherence tomography scans accurately classifies glaucoma suspects. J. Glaucoma 26:1086–94 [PubMed: 29045329]

Mwanza J-C, Chang RT, Budenz DL, Durbin MK, Gendy MG, et al. 2010. Reproducibility of peripapillary retinal nerve fiber layer thickness and optic nerve head parameters measured with Cirrus HD-OCT in glaucomatous eyes. Investig. Ophthalmol. Vis. Sci 51:5724–30 [PubMed: 20574014]

Mwanza J-C, Durbin MK, Budenz DL, Sayyad FE, Chang RT, et al. 2012a. Glaucoma diagnostic accuracy of ganglion cell-inner plexiform layer thickness: comparison with nerve fiber layer and optic nerve head. Ophthalmology 119:1151–58 [PubMed: 22365056]

Mwanza J-C, Oakley JD, Budenz DL, Anderson DR, Cirrus Optical Coherence Tomography Normative Database Study Group. 2011. Ability of Cirrus HD-OCT optic nerve head parameters to discriminate normal from glaucomatous eyes. Ophthalmology 118:241–48.e1 [PubMed: 20920824]

Mwanza J-C, Sayyad FE, Aref AA, Budenz DL. 2012b. Rates of abnormal retinal nerve fiber layer and ganglion cell layer OCT scans in healthy myopic eyes: Cirrus versus RTVue. Ophthalmic Surg. Lasers Imaging 43:S67–74 [PubMed: 23357327]

Na JH, Sung KR, Baek S, Kim YJ, Durbin MK, et al. 2012. Detection of glaucoma progression by assessment of segmented macular thickness data obtained using spectral domain optical coherence tomography. Investig. Ophthalmol. Vis. Sci 53:3817–26 [PubMed: 22562510]

Na JH, Sung KR, Lee JR, Lee KS, Baek S, et al. 2013. Detection of glaucomatous progression by spectral-domain optical coherence tomography. Ophthalmology 120:1388–95 [PubMed: 23474248]

Nadler Z, Wang B, Wollstein G, Nevins JE, Ishikawa H, et al. 2014. Repeatability of in vivo 3D lamina cribrosa microarchitecture using adaptive optics spectral domain optical coherence tomography. Biomed. Opt. Express 5:1114–23 [PubMed: 24761293]

Naghizadeh F, Garas A, Vargha P, Holló G. 2014. Detection of early glaucomatous progression with different parameters of the RTVue optical coherence tomograph. J. Glaucoma 23:195–98 [PubMed: 22922666]

Nicolela MT, Hnik P, Schulzer M, Drance SM. 1997. Reproducibility of retinal and optic nerve head blood flow measurements with scanning laser Doppler flowmetry. J. Glaucoma 6:157–64 [PubMed: 9211138]

Nirmaier T, Pudasaini G, Bille J. 2003. Very fast wave-front measurements at the human eye with a custom CMOS-based Hartmann-Shack sensor. Opt. Express 11:2704–16 [PubMed: 19471385]

Niwas SI, Lin W, Kwoh CK, Kuo CC, Sng CC, et al. 2016. Cross-examination for angle-closure glaucoma feature detection. IEEE J. Biomed. Health Inform 20:343–54 [PubMed: 25561599]

Nuyen B, Mansouri K, Weinreb RN. 2012. Imaging of the lamina cribrosa using swept-source optical coherence tomography. J. Curr. Glaucoma Pract 6:113–19 [PubMed: 26997766]

Oddone F, Lucenteforte E, Michelessi M, Rizzo S, Donati S, et al. 2016. Macular versus retinal nerve fiber layer parameters for diagnosing manifest glaucoma: a systematic review of diagnostic accuracy studies. Ophthalmology 123:939–49 [PubMed: 26891880]

Olafsdottir OB, Hardarson SH, Gottfredsdottir MS, Harris A, Stefánsson E. 2011. Retinal oximetry in primary open-angle glaucoma. Investig. Ophthalmol. Vis. Sci 52:6409–13 [PubMed: 21715353]

Olafsdottir OB, Vandewalle E, Abegão Pinto L, Geirsdottir A, De Clerck E, et al. 2014. Retinal oxygen metabolism in healthy subjects and glaucoma patients. Br. J. Ophthalmol 98:329–33 [PubMed: 24403567]

Ou Y, Jo RE, Ullian EM, Wong RO, Della Santina L. 2016. Selective vulnerability of specific retinal ganglion cell types and synapses after transient ocular hypertension. J. Neurosci 36:9240–52 [PubMed: 27581463]

Park HL, Kim JW, Park CK. 2018. Choroidal microvasculature dropout is associated with progressive retinal nerve fiber layer thinning in glaucoma with disc hemorrhage. Ophthalmology 125:1003–13 [PubMed: 29486903]

Park JH, Yoo C, Girard MJA, Mari JM, Kim YY. 2018. Peripapillary vessel density in glaucomatous eyes: comparison between pseudoexfoliation glaucoma and primary open-angle glaucoma. J. Glaucoma 27:1009–16 [PubMed: 30134370]

Park K, Kim J, Lee J. 2018. Macular vessel density and ganglion cell/inner plexiform layer thickness and their combinational index using artificial intelligence. J. Glaucoma 27:750–60 [PubMed: 30005033]

Patel RC, Wang J, Hwang TS, Zhang M, Gao SS, et al. 2018. Plexus-specific detection of retinal vascular pathologic conditions with projection-resolved OCT angiography. Ophthalmol. Retina 2:816–26 [PubMed: 30148244]

Paunescu LA, Schuman JS, Price LL, Stark PC, Beaton S, et al. 2004. Reproducibility of nerve fiber thickness, macular thickness, and optic nerve head measurements using StratusOCT. Investig. Ophthalmol. Vis. Sci 45:1716–24 [PubMed: 15161831]

Penteado RC, Zangwill LM, Daga FB, Saunders LJ, Manalastas PIC, et al. 2018. Optical coherence tomography angiography macular vascular density measurements and the central 10–2 visual field in glaucoma. J. Glaucoma 27:481–89 [PubMed: 29664832]

Phene S, Dunn RC, Hammel N, Liu Y, Krause J, et al. 2019. Deep learning and glaucoma specialists: the relative importance of optic disc features to predict glaucoma referral in fundus photographs. Ophthalmology 126:1627–39 [PubMed: 31561879]

Philip S, Najafi A, Tantraworasin A, Chui TYP, Rosen RB, Ritch R. 2019. Macula vessel density and foveal avascular zone parameters in exfoliation glaucoma compared to primary open-angle glaucoma. Investig. Ophthalmol. Vis. Sci 60:1244–53 [PubMed: 30924849]

Pi S, Camino A, Cepurna W, Wei X, Zhang M, et al. 2018. Automated spectroscopic retinal oximetry with visible-light optical coherence tomography. Biomed. Opt. Express 9:2056–67 [PubMed: 29760969]

Piltz-Seymour JR. 1999. Laser Doppler flowmetry of the optic nerve head in glaucoma. Surv. Ophthalmol 43(Suppl. 1):S191–98 [PubMed: 10416763]

Poplin R, Varadarajan AV, Blumer K, Liu Y, McConnell MV, et al. 2018. Prediction of cardiovascular risk factors from retinal fundus photographs via deep learning. Nat. Biomed. Eng 2:158–64 [PubMed: 31015713]

Popovic Z, Knutsson P, Thaung J, Owner-Petersen M, Sjöstrand J. 2011. Noninvasive imaging of human foveal capillary network using dual-conjugate adaptive optics. Investig. Ophthalmol. Vis. Sci 52:2649–55 [PubMed: 21228372]

Porter J, Guirao A, Cox IG, Williams DR. 2001. Monochromatic aberrations of the human eye in a large population. J. Opt. Soc. Am. A Opt. Image Sci. Vis 18:1793–803 [PubMed: 11488483]

Potsaid B, Gorczynska I, Srinivasan VJ, Chen Y, Jiang J, et al. 2008. Ultrahigh speed spectral / Fourier domain OCT ophthalmic imaging at 70,000 to 312,500 axial scans per second. Opt. Express 16:15149–69 [PubMed: 18795054]

Povazay B, Apolonski A, Unterhuber A, Hermann B, Bizheva K, et al. 2002. Visible light optical coherence tomography. Proc. SPIE 4619, Coherence Domain Opt. Methods Biomed. Sci. Clin. Appl. VI. 10.1117/12.470466

Pradhan ZS, Dixit S, Sreenivasaiah S, Rao HL, Venugopal JP, et al. 2018. A sectoral analysis of vessel density measurements in perimetrically intact regions of glaucomatous eyes: an optical coherence tomography angiography study. J. Glaucoma 27:525–31 [PubMed: 29557826]

Prünte C, Flammer J, Markstein R, Rudin M. 1995. Quantification of optic nerve blood flow changes using magnetic resonance imaging. Investig. Ophthalmol. Vis. Sci 36:247–51 [PubMed: 7822153]

Puliafito CA, Hee MR, Lin CP, Reichel E, Schuman JS, et al. 1995. Imaging of macular diseases with optical coherence tomography. Ophthalmology 102:217–29 [PubMed: 7862410]

Quigley HA, Addicks EM, Green WR, Maumenee AE. 1981. Optic nerve damage in human glaucoma. II. The site of injury and susceptibility to damage. Arch. Ophthalmol 99:635–49 [PubMed: 6164357]

Quigley HA, Anderson DR. 1977. Distribution of axonal transport blockade by acute intraocular pressure elevation in the primate optic nerve head. Investig. Ophthalmol. Vis. Sci 16:640–44 [PubMed: 68942]

Quigley HA, Broman AT. 2006. The number of people with glaucoma worldwide in 2010 and 2020. Br. J. Ophthalmol 90:262–67 [PubMed: 16488940]

Radius RL, Anderson DR. 1981. Rapid axonal transport in primate optic nerve. Distribution of pressure-induced interruption. Arch. Ophthalmol 99:650–54 [PubMed: 6164358]

Ramaswamy G, Lombardo M, Devaney N. 2014. Registration of adaptive optics corrected retinal nerve fiber layer (RNFL) images. Biomed. Opt. Express 5:1941–51 [PubMed: 24940551]

Rankin SJ. 1999. Color Doppler imaging of the retrobulbar circulation in glaucoma. Surv. Ophthalmol 43(Suppl. 1):S176–82 [PubMed: 10416761]

Rao HL, Kadambi SV, Weinreb RN, Puttaiah NK, Pradhan ZS, et al. 2017a. Diagnostic ability of peripapillary vessel density measurements of optical coherence tomography angiography in primary open-angle and angle-closure glaucoma. Br. J. Ophthalmol 101:1066–70 [PubMed: 27899368]

Rao HL, Pradhan ZS, Weinreb RN, Dasari S, Riyazuddin M, et al. 2017b. Relationship of optic nerve structure and function to peripapillary vessel density measurements of optical coherence tomography angiography in glaucoma. J. Glaucoma 26:548–54 [PubMed: 28333896]

Rao HL, Pradhan ZS, Weinreb RN, Reddy HB, Riyazuddin M, et al. 2017c. Determinants of peripapillary and macular vessel densities measured by optical coherence tomography angiography in normal eyes. J. Glaucoma 26:491–97 [PubMed: 28263261]

Rao HL, Pradhan ZS, Weinreb RN, Riyazuddin M, Dasari S, et al. 2017d. A comparison of the diagnostic ability of vessel density and structural measurements of optical coherence tomography in primary open angle glaucoma. PLOS ONE 12:e0173930 [PubMed: 28288185]

Rao HL, Pradhan ZS, Weinreb RN, Riyazuddin M, Dasari S, et al. 2017e. Vessel density and structural measurements of optical coherence tomography in primary angle closure and primary angle closure glaucoma. Am. J. Ophthalmol 177:106–15 [PubMed: 28254626]

Rao HL, Riyazuddin M, Dasari S, Puttaiah NK, Pradhan ZS, et al. 2018. Relationship of macular thickness and function to optical microangiography measurements in glaucoma. J. Glaucoma 27:210–18 [PubMed: 29329138]

Rojas CD, Reed DM, Moroi SE. 2020. Usefulness of iCare HOME in telemedicine workflow to detect real-world intraocular pressure response to glaucoma medication change. Ophthalmol. Glaucoma 3(5):403–5 [PubMed: 32980045]

Sakaguchi K, Higashide T, Udagawa S, Ohkubo S, Sugiyama K. 2017. Comparison of sectoral structure-function relationships in glaucoma: vessel density versus thickness in the peripapillary retinal nerve fiber layer. Investig. Ophthalmol. Vis. Sci 58:5251–62 [PubMed: 29049726]

Schuman JS. 2008. Spectral domain optical coherence tomography for glaucoma (an AOS thesis). Trans. Am. Ophthalmol. Soc 106:426–58 [PubMed: 19277249]

Schuman JS. 2016. Optical coherence tomography in high myopia. JAMA Ophthalmol 134:1040 [PubMed: 27441781]

Schuman JS, Hee MR, Arya AV, Pedut-Kloizman T, Puliafito CA, et al. 1995. Optical coherence tomography: a new tool for glaucoma diagnosis. Curr. Opin. Ophthalmol 6:89–95 [PubMed: 10150863]

Scripsema NK, Garcia PM, Bavier RD, Chui TY, Krawitz BD, et al. 2016. Optical coherence tomography angiography analysis of perfused peripapillary capillaries in primary open-angle glaucoma and normal-tension glaucoma. Investig. Ophthalmol. Vis. Sci 57:OCT611–20 [PubMed: 27742922]

Sehi M, Grewal DS, Sheets CW, Greenfield DS. 2009. Diagnostic ability of Fourier-domain versus time-domain optical coherence tomography for glaucoma detection. Am. J. Ophthalmol 148:597–605 [PubMed: 19589493]

Shiga Y, Kunikata H, Aizawa N, Kiyota N, Maiya Y, et al. 2016. Optic nerve head blood flow, as measured by laser speckle flowgraphy, is significantly reduced in preperimetric glaucoma. Curr. Eye Res 41:1447–53 [PubMed: 27159148]

Shin JW, Kwon J, Lee J, Kook MS. 2019. Relationship between vessel density and visual field sensitivity in glaucomatous eyes with high myopia. Br. J. Ophthalmol 103:585–91

Shoji T, Zangwill LM, Akagi T, Saunders LJ, Yarmohammadi A, et al. 2017. Progressive macula vessel density loss in primary open-angle glaucoma: a longitudinal study. Am. J. Ophthalmol 182:107–17 [PubMed: 28734815]

Shu X, Beckmann L, Wang Y, Rubinoff I, Lucy K, et al. 2019. Designing visible-light optical coherence tomography towards clinics. Quant. Imaging Med. Surg 9:769–81 [PubMed: 31281773]

Shu X, Beckmann L, Zhang H. 2017. Visible-light optical coherence tomography: a review. J. Biomed. Opt 22:1–14

Sigal IA, Ethier CR. 2009. Biomechanics of the optic nerve head. Exp. Eye Res 88:799–807 [PubMed: 19217902]

Sigal IA, Wang B, Strouthidis NG, Akagi T, Girard MJ. 2014. Recent advances in OCT imaging of the lamina cribrosa. Br. J. Ophthalmol 98(Suppl. 2):ii34–39 [PubMed: 24934221]

Sommer A, Katz J, Quigley HA, Miller NR, Robin AL, et al. 1991. Clinically detectable nerve fiber atrophy precedes the onset of glaucomatous field loss. Arch. Ophthalmol 109:77–83 [PubMed: 1987954]

Sommer A, Miller NR, Pollack I, Maumenee AE, George T. 1977. The nerve fiber layer in the diagnosis of glaucoma. Arch. Ophthalmol 95:2149–56 [PubMed: 588106]

Song W, Wei Q, Jiao S, Zhang HF. 2013. Integrated photoacoustic ophthalmoscopy and spectral-domain optical coherence tomography. J. Vis. Exp 71:e4390

Song W, Wei Q, Liu W, Liu T, Yi J, et al. 2014. A combined method to quantify the retinal metabolic rate of oxygen using photoacoustic ophthalmoscopy and optical coherence tomography. Sci. Rep 4:6525 [PubMed: 25283870]

Spaide RF, Fujimoto JG, Waheed NK. 2015. Image artifacts in optical coherence tomography angiography. Retina 35:2163–80 [PubMed: 26428607]

Spaide RF, Koizumi H, Pozzoni MC. 2008. Enhanced depth imaging spectral-domain optical coherence tomography. Am. J. Ophthalmol 146:496–500 [PubMed: 18639219]

Suh MH, Park JW, Kim HR. 2018. Association between the deep-layer microvasculature dropout and the visual field damage in glaucoma. J. Glaucoma 27:543–51 [PubMed: 29613982]

Suh MH, Zangwill LM, Manalastas PI, Belghith A, Yarmohammadi A, et al. 2016. Deep retinal layer microvasculature dropout detected by the optical coherence tomography angiography in glaucoma. Ophthalmology 123:2509–18 [PubMed: 27769587]

Sung KR, Na JH, Lee Y. 2012a. Glaucoma diagnostic capabilities of optic nerve head parameters as determined by Cirrus HD optical coherence tomography. J. Glaucoma 21:498–504 [PubMed: 21637115]

Sung KR, Sun JH, Na JH, Lee JY, Lee Y. 2012b. Progression detection capability of macular thickness in advanced glaucomatous eyes. Ophthalmology 119:308–13 [PubMed: 22182800]

Sung KR, Wollstein G, Kim NR, Na JH, Nevins JE, et al. 2012c. Macular assessment using optical coherence tomography for glaucoma diagnosis. Br. J. Ophthalmol 96:1452–55 [PubMed: 23018425]

Suwan Y, Geyman LS, Fard MA, Tantraworasin A, Chui TY, et al. 2018. Peripapillary perfused capillary density in exfoliation syndrome and exfoliation glaucoma versus POAG and healthy controls: an OCTA study. Asia Pac. J. Ophthalmol 7:84–89

Swanson EA, Fujimoto JG. 2017. The ecosystem that powered the translation of OCT from fundamental research to clinical and commercial impact [Invited]. Biomed. Opt. Express 8:1638–64 [PubMed: 28663854]

Takagi D, Sawada A, Yamamoto T. 2017. Evaluation of a new rebound self-tonometer, Icare HOME: comparison with Goldmann applanation tonometer. J. Glaucoma 26:613–18 [PubMed: 28369004]

Takayama K, Hangai M, Durbin M, Nakano N, Morooka S, et al. 2012. A novel method to detect local ganglion cell loss in early glaucoma using spectral-domain optical coherence tomography. Investig. Ophthalmol. Vis. Sci 53:6904–13 [PubMed: 22977136]

Takayama K, Hangai M, Kimura Y, Morooka S, Nukada M, et al. 2013. Three-dimensional imaging of lamina cribrosa defects in glaucoma using swept-source optical coherence tomography. Investig. Ophthalmol. Vis. Sci 54:4798–807 [PubMed: 23778878]

Tezel G, Wax MB. 2004. Hypoxia-inducible factor 1α in the glaucomatous retina and optic nerve head. Arch. Ophthalmol 122:1348–56 [PubMed: 15364715]

Thibos LN, Hong X, Bradley A, Cheng X. 2002. Statistical variation of aberration structure and image quality in a normal population of healthy eyes. J. Opt. Soc. Am. A Opt. Image Sci. Vis 19:2329–48 [PubMed: 12469728]

Thompson AC, Jammal AA, Berchuck SI, Mariottoni EB, Medeiros FA. 2020. Assessment of a segmentation-free deep learning algorithm for diagnosing glaucoma from optical coherence tomography scans. JAMA Ophthalmol 138(4):333–39 [PubMed: 32053142]

Ting DSW, Cheung CY, Lim G, Tan GSW, Quang ND, et al. 2017. Development and validation of a deep learning system for diabetic retinopathy and related eye diseases using retinal images from multiethnic populations with diabetes. JAMA 318:2211–23 [PubMed: 29234807]

Torti C, Považay B, Hofer B, Unterhuber A, Carroll J, et al. 2009. Adaptive optics optical coherence tomography at 120,000 depth scans/s for non-invasive cellular phenotyping of the living human retina. Opt. Express 17:19382–400 [PubMed: 19997159]

Triolo G, Rabiolo A, Shemonski ND, Fard A, Di Matteo F, et al. 2017. Optical coherence tomography angiography macular and peripapillary vessel perfusion density in healthy subjects, glaucoma suspects, and glaucoma patients. Investig. Ophthalmol. Vis. Sci 58:5713–22 [PubMed: 29114838]

Umfress AC, Brantley MA Jr. 2016. Eye care disparities and health-related consequences in elderly patients with age-related eye disease. Semin. Ophthalmol 31:432–38 [PubMed: 27116323]

van der Schoot J, Vermeer KA, de Boer JF, Lemij HG. 2012. The effect of glaucoma on the optical attenuation coefficient of the retinal nerve fiber layer in spectral domain optical coherence tomography images. Investig. Ophthalmol. Vis. Sci 53:2424–30 [PubMed: 22427540]

Vandewalle E, Abegão Pinto L, Olafsdottir OB, De Clerck E, Stalmans P, et al. 2014. Oximetry in glaucoma: correlation of metabolic change with structural and functional damage. Acta Ophthalmol 92:105–10 [PubMed: 23323611]

Venugopal JP, Rao HL, Weinreb RN, Dasari S, Riyazuddin M, et al. 2019. Repeatability and comparability of peripapillary vessel density measurements of high-density and non-high-density optical coherence tomography angiography scans in normal and glaucoma eyes. Br. J. Ophthalmol 103:949–54 [PubMed: 30120128]

Venugopal JP, Rao HL, Weinreb RN, Pradhan ZS, Dasari S, et al. 2018. Repeatability of vessel density measurements of optical coherence tomography angiography in normal and glaucoma eyes. Br. J. Ophthalmol 102:352–57 [PubMed: 28739645]

Vidotti VG, Costa VP, Silva FR, Resende GM, Cremasco F, et al. 2013. Sensitivity and specificity of machine learning classifiers and spectral domain OCT for the diagnosis of glaucoma. Eur. J. Ophthalmol 23:61–69

Vilupuru AS, Rangaswamy NV, Frishman LJ, Smith EL 3rd, Harwerth RS, Roorda A. 2007. Adaptive optics scanning laser ophthalmoscopy for in vivo imaging of lamina cribrosa. J. Opt. Soc. Am. A Opt. Image Sci. Vis 24:1417–25 [PubMed: 17429488]

Wan KH, Lam AKN, Leung CK-S. 2018. Optical coherence tomography angiography compared with optical coherence tomography macular measurements for detection of glaucoma. JAMA Ophthalmol 136:866–74 [PubMed: 29852029]

Wang B, Nevins JE, Nadler Z, Wollstein G, Ishikawa H, et al. 2013. In vivo lamina cribrosa micro-architecture in healthy and glaucomatous eyes as assessed by optical coherence tomography. Investig. Ophthalmol. Vis. Sci 54:8270–74 [PubMed: 24302585]

Wang B, Tran H, Smith MA, Kostanyan T, Schmitt SE, et al. 2017. In-vivo effects of intraocular and intracranial pressures on the lamina cribrosa microstructure. PLOS ONE 12:e0188302 [PubMed: 29161320]

Wang SY, Singh K, Lin SC. 2012. Prevalence and predictors of depression among participants with glaucoma in a nationally representative population sample. Am. J. Ophthalmol 154:436–44.e2 [PubMed: 22789562]

Wang X, Jiang C, Ko T, Kong X, Yu X, et al. 2015. Correlation between optic disc perfusion and glaucomatous severity in patients with open-angle glaucoma: an optical coherence tomography angiography study. Graefes Arch. Clin. Exp. Ophthalmol 253:1557–64 [PubMed: 26255817]

Wang Y, Fawzi AA, Varma R, Sadun AA, Zhang X, et al. 2011. Pilot study of optical coherence tomography measurement of retinal blood flow in retinal and optic nerve diseases. Investig. Ophthalmol. Vis. Sci 52:840–45 [PubMed: 21051715]

Weinreb RN, Leung CKS, Crowston JG, Medeiros FA, Friedman DS, et al. 2016. Primary open-angle glaucoma. Nat. Rev. Dis. Primers 2:16067 [PubMed: 27654570]

Werner AC, Shen LQ. 2019. A review of OCT angiography in glaucoma. Semin. Ophthalmol 34:279–86 [PubMed: 31158045]

Werner JS, Keltner JL, Zawadzki RJ, Choi SS. 2011. Outer retinal abnormalities associated with inner retinal pathology in nonglaucomatous and glaucomatous optic neuropathies. Eye 25:279–89 [PubMed: 21293495]

Wessel JM, Horn FK, Tornow RP, Schmid M, Mardin CY, et al. 2013. Longitudinal analysis of progression in glaucoma using spectral-domain optical coherence tomography. Investig. Ophthalmol. Vis. Sci 54:3613–20 [PubMed: 23633657]

White B, Pierce M, Nassif N, Cense B, Park B, et al. 2003. In vivo dynamic human retinal blood flow imaging using ultra-high-speed spectral domain optical coherence tomography. Opt. Express 11:3490–97 [PubMed: 19471483]

Wieser W, Biedermann BR, Klein T, Eigenwillig CM, Huber R. 2010. Multi-megahertz OCT: high quality 3D imaging at 20 million A-scans and 4.5 GVoxels per second. Opt. Express 18:14685–704 [PubMed: 20639955]

Williams DR. 2011. Imaging single cells in the living retina. Vis. Res 51:1379–96 [PubMed: 21596053]

Wollstein G, Schuman JS, Price LL, Aydin A, Beaton SA, et al. 2004. Optical coherence tomography (OCT) macular and peripapillary retinal nerve fiber layer measurements and automated visual fields. Am. J. Ophthalmol 138:218–25 [PubMed: 15289130]

Wollstein G, Schuman JS, Price LL, Aydin A, Stark PC, et al. 2005. Optical coherence tomography longitudinal evaluation of retinal nerve fiber layer thickness in glaucoma. Arch. Ophthalmol 123:464–70 [PubMed: 15824218]

Xu BY, Chiang M, Chaudhary S, Kulkarni S, Pardeshi AA, Varma R. 2019. Deep learning classifiers for automated detection of gonioscopic angle closure based on anterior segment OCT images. Am. J. Ophthalmol 208:273–80 [PubMed: 31445003]

Xu Y, Liu J, Cheng J, Lee BH, Wong DW, et al. 2013. Automated anterior chamber angle localization and glaucoma type classification in OCT images. Conf. Proc. IEEE Eng. Med. Biol. Soc 2013:7380–83

Yarmohammadi A, Zangwill LM, Diniz-Filho A, Saunders LJ, Suh MH, et al. 2017. Peripapillary and macular vessel density in patients with glaucoma and single-hemifield visual field defect. Ophthalmology 124:709–19 [PubMed: 28196732]

Yarmohammadi A, Zangwill LM, Diniz-Filho A, Suh MH, Yousefi S, et al. 2016. Relationship between optical coherence tomography angiography vessel density and severity of visual field loss in glaucoma. Ophthalmology 123:2498–508 [PubMed: 27726964]

Yi J, Chen S, Backman V, Zhang HF. 2014. In vivo functional microangiography by visible-light optical coherence tomography. Biomed. Opt. Express 5:3603–12 [PubMed: 25360376]

Yi J, Liu W, Chen S, Backman V, Sheibani N, et al. 2015. Visible light optical coherence tomography measures retinal oxygen metabolic response to systemic oxygenation. Light Sci. Appl 4:e334 [PubMed: 26658555]

You JY, Park SC, Su D, Teng CC, Liebmann JM, Ritch R. 2013. Focal lamina cribrosa defects associated with glaucomatous rim thinning and acquired pits. JAMA Ophthalmol 131:314–20 [PubMed: 23370812]

Yousefi S, Kiwaki T, Zheng Y, Sugiura H, Asaoka R, et al. 2018. Detection of longitudinal visual field progression in glaucoma using machine learning. Am. J. Ophthalmol 193:71–79 [PubMed: 29920226]

Yun S, Tearney G, de Boer J, Iftimia N, Bouma B. 2003. High-speed optical frequency-domain imaging. Opt. Express 11:2953–63 [PubMed: 19471415]

Zangwill LM, Chan K, Bowd C, Hao J, Lee TW, et al. 2004. Heidelberg retina tomograph measurements of the optic disc and parapapillary retina for detecting glaucoma analyzed by machine learning classifiers. Investig. Ophthalmol. Vis. Sci 45:3144–51 [PubMed: 15326133]

Zeimer R, Asrani S, Zou S, Quigley H, Jampel H. 1998. Quantitative detection of glaucomatous damage at the posterior pole by retinal thickness mapping. A pilot study. Ophthalmology 105:224–31 [PubMed: 9479279]

Zhang A, Zhang Q, Chen CL, Wang RK. 2015. Methods and algorithms for optical coherence tomography-based angiography: a review and comparison. J. Biomed. Opt 20:100901 [PubMed: 26473588]

Zhang HF, Maslov K, Stoica G, Wang LV. 2006. Functional photoacoustic microscopy for high-resolution and noninvasive in vivo imaging. Nat. Biotechnol 24:848–51 [PubMed: 16823374]

Zhang S, Wu C, Liu L, Jia Y, Zhang Y, et al. 2017. Optical coherence tomography angiography of the peripapillary retina in primary angle-closure glaucoma. Am. J. Ophthalmol 182:194–200 [PubMed: 28797550]

Zhang T, Kho AM, Srinivasan VJ. 2019. Improving visible light OCT of the human retina with rapid spectral shaping and axial tracking. Biomed. Opt. Express 10:2918–31 [PubMed: 31259062]

Zhang X, Dastiridou A, Francis BA, Tan O, Varma R, et al. 2017. Comparison of glaucoma progression detection by optical coherence tomography and visual field. Am. J. Ophthalmol 184:63–74 [PubMed: 28964806]

Zhang X, Hu J, Knighton RW, Huang X-R, Puliafito CA, Jiao S. 2011. Dual-band spectral-domain optical coherence tomography for in vivo imaging the spectral contrasts of the retinal nerve fiber layer. Opt. Express 19:19653–59 [PubMed: 21996906]

Zheng C, Johnson TV, Garg A, Boland MV. 2019. Artificial intelligence in glaucoma. Curr. Opin. Ophthalmol 30:97–103 [PubMed: 30562242]

Zhou B, Khosla A, Lapedriza A, Oliva A, Torralba A. 2016. Learning deep features for discriminative localization Paper presented at 2016 IEEE Conference on Computer Vision and Pattern Recognition, Las Vegas, NV, June 27–30

SUMMARY POINTS

1. Glaucoma is a progressive, degenerative disease that can lead to irreversible blindness. Through its development from time-domain optical coherence tomography (TD-OCT) to spectral-domain OCT (SD-OCT) and swept-source OCT (SS-OCT), and improvements in resolution and scan speeds, OCT imaging has become a powerful tool for diagnosing and detecting the progression of glaucoma.
2. The lamina cribrosa (LC) is the primary site of glaucomatous retinal ganglion cell axonal injury. The LC microstructure can be an OCT imaging biomarker for glaucoma.
3. The integration of adaptive optics with OCT has further improved the ability to image the optic nerve head and the retina with high axial and transverse resolution. It is possible to discriminate individual photoreceptors, retinal nerve fiber layer (RNFL) axon bundles, and the LC microstructure, providing more ways to sensitively detect and monitor glaucoma.
4. Vascular dysfunction can be a contributor to the development and progression of glaucoma. OCT-angiography (OCTA) is a noninvasive technique for specifically assessing the retinal and optic nerve circulation, with high resolution and reproducibility. OCTA-derived quantitative measurements of ocular vasculature such as vessel density and flow index have shown evidence for vascular compromise in glaucomatous eyes and have diagnostic capabilities comparable to conventional OCT parameters.
5. Visible-light OCT (Vis-OCT) utilizes light of shorter wavelengths compared with conventional OCT systems, which use near-IR light. As a result, Vis-OCT can offer new imaging biomarkers for glaucoma, such as visualization of the retinal inner plexiform sublayers. Vis-OCT can also assess in vivo oxygen saturation using vascular spectroscopic OCT signals.
6. Automation of tasks with artificial intelligence (AI) algorithms, utilizing OCT parameters and more complex inputs such as raw OCT imaging data, has performed well in the diagnosis of glaucoma. AI can also provide insight into structural regions that have yet to be established as having value in glaucoma detection and management.
7. While OCT technology has its limitations, it is constantly evolving. Intraoperative OCT and teleophthalmology with the development of home OCT devices are two ways in which OCT technology can profoundly impact glaucoma management in the future.

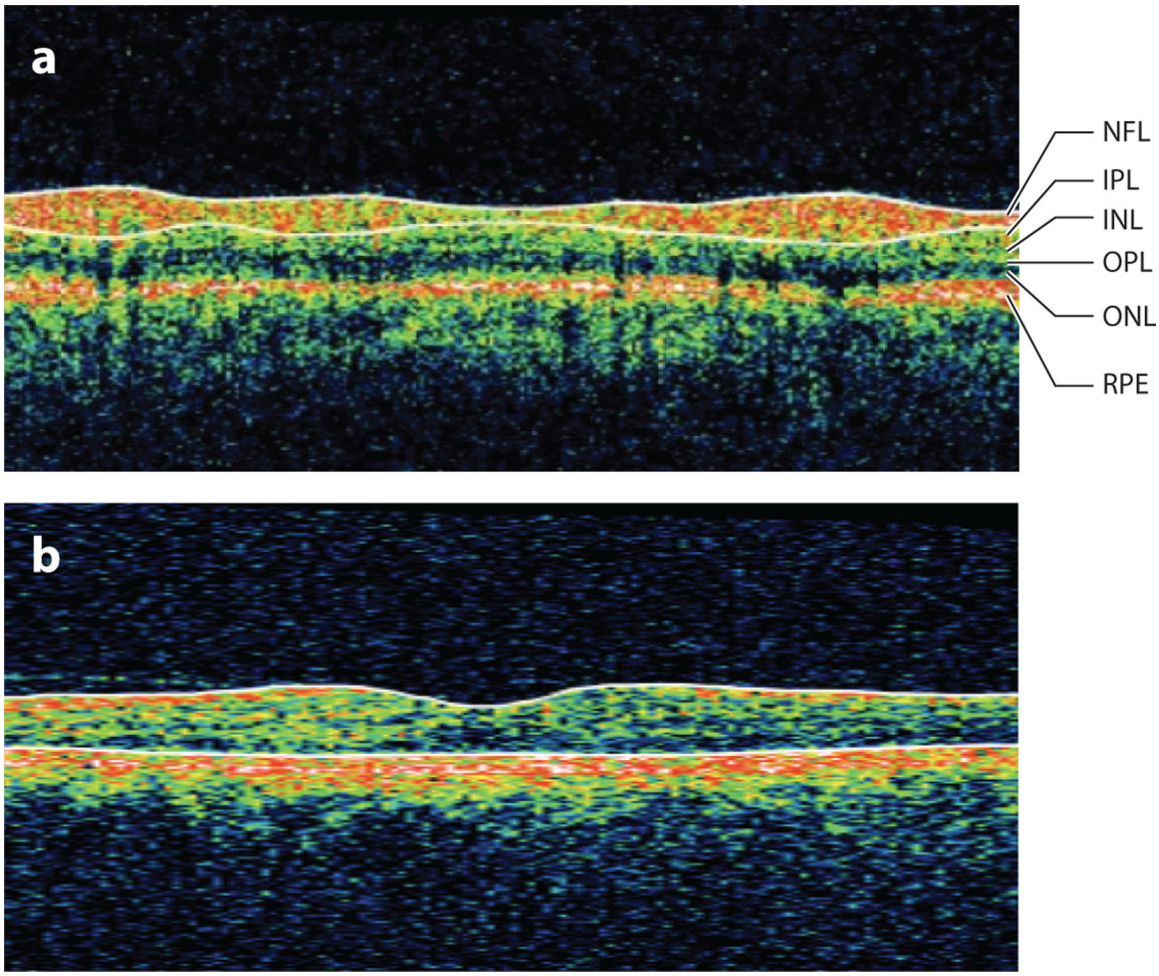

Figure 1.

Stratus-OCT (Carl Zeiss Meditec, Dublin, California) B-scan of (*a*) the peripapillary retina with retinal layers labeled and (*b*) the macular retina. Abbreviations: INL, inner nuclear layer; IPL, inner plexiform layer; NFL, nerve fiber layer; OCT, optical coherence tomography; ONL, outer nuclear layer; OPL, outer plexiform layer; RPE, retinal pigment epithelium.

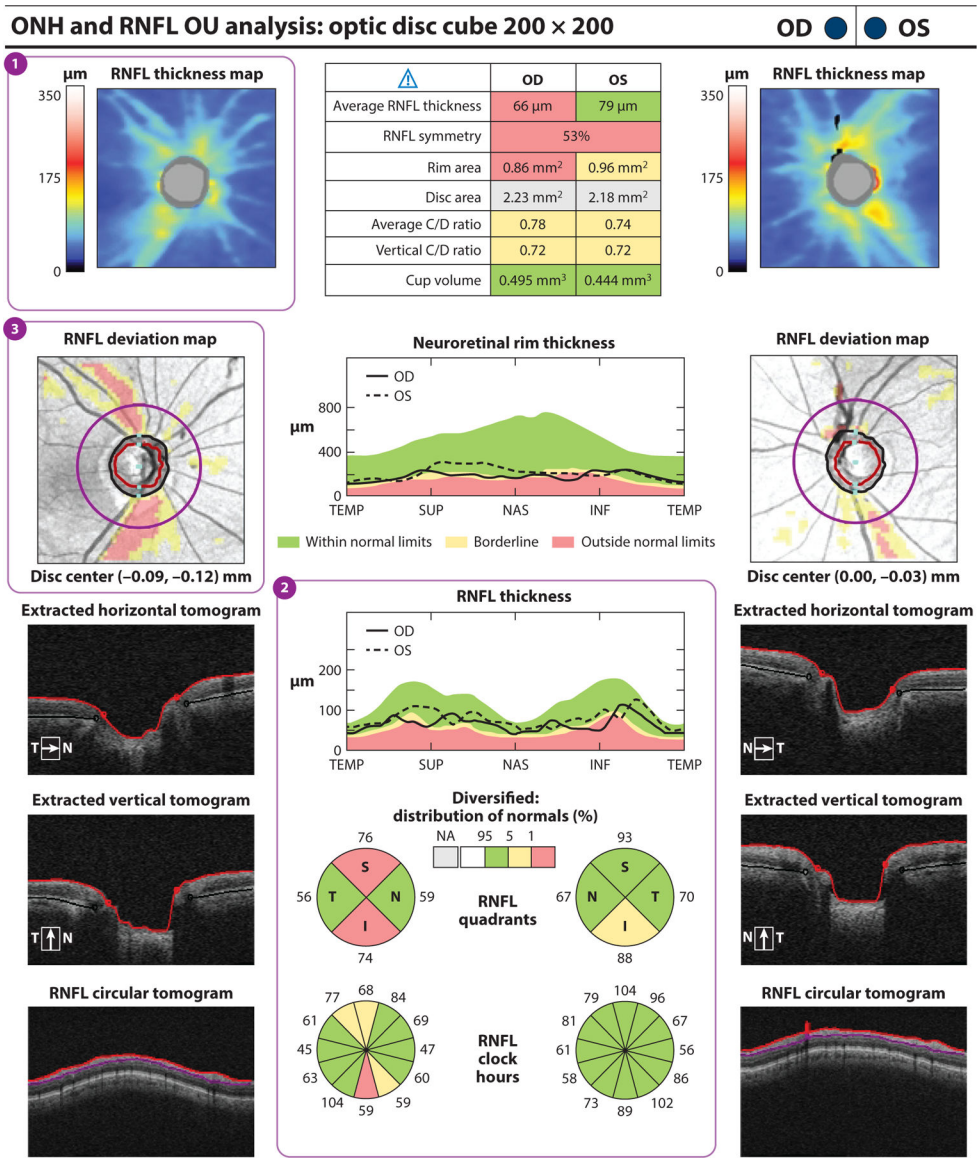

Figure 2.

Cirrus HD-OCT (Carl Zeiss Meditec, Dublin, California) report for a subject with one glaucomatous eye (OD) and one nonglaucomatous eye (OS). (*a*) The RNFL thickness map (①) displays RNFL thickness around the optic disc through a color map, with the thicker RNFL measurements in red and yellow and the thinner RNFL measurements in green and blue. RNFL thickness measurements by quadrant (S, I, N, and T) and clock hour are shown. (②) Values within the normal range of age-matched controls are in green (within normal limits). Values that fall outside the normal range for their age are displayed in yellow if $p < 5\%$ and $\geq 1\%$ (borderline) or in red if $p < 1\%$ (outside normal limits). RNFL thickness in the superior and inferior quadrants is abnormal in OD compared with OS, in which the inferior quadrant is borderline. The RNFL deviation map (③) shows RNFL thickness deviations from the normative database overlaid on an en face image. Borderline RNFL thickness measurements are shown in yellow, and RNFL thicknesses outside normal limits

are shown in red. Substantial glaucomatous thinning is seen in red OD. Abbreviations: C/D ratio, cup-to-disc ratio; HD-OCT, high-definition optical coherence tomography; I, inferior; N, nasal; NA, not applicable; ONH, optic nerve head; RNFL, retinal nerve fiber layer; S, superior; T, temporal.

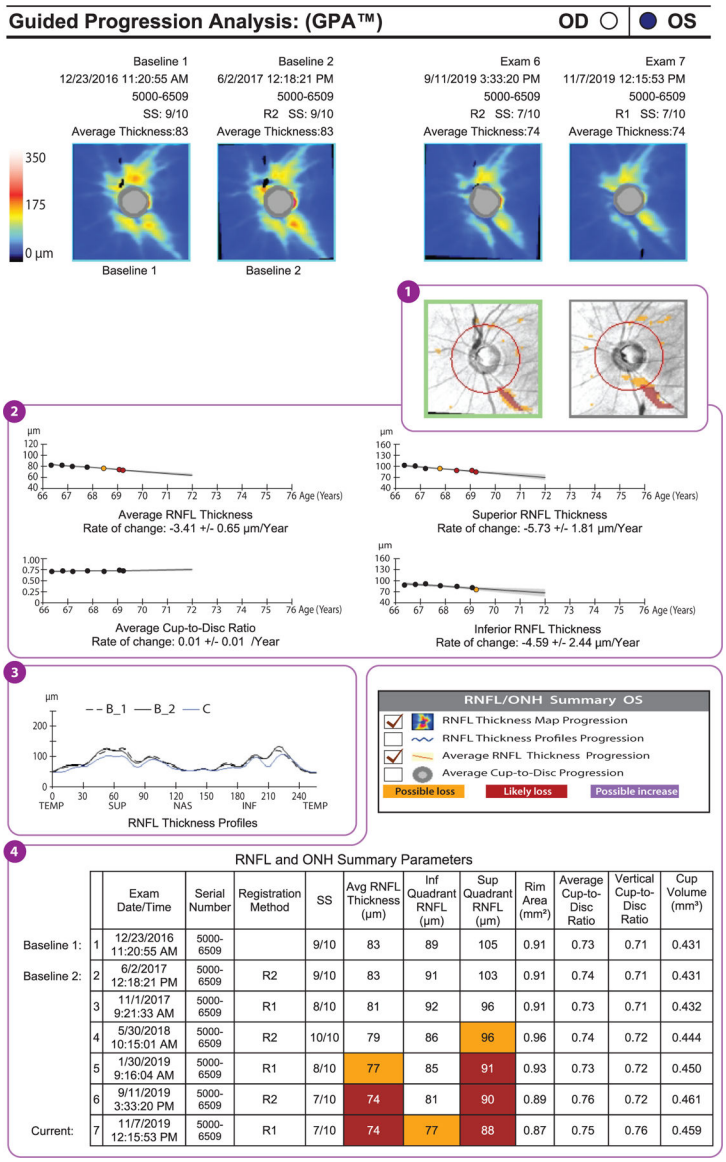

		Exam Date/Time	Serial Number	Registration Method	SS	Avg RNFL Thickness (µm)	Inf Quadrant RNFL (µm)	Sup Quadrant RNFL (µm)	Rim Area (mm²)	Average Cup-to-Disc Ratio	Vertical Cup-to-Disc Ratio	Cup Volume (mm³)
Baseline 1:	1	12/23/2016 11:20:55 AM	5000-6509		9/10	83	89	105	0.91	0.73	0.71	0.431
Baseline 2:	2	6/2/2017 12:18:21 PM	5000-6509	R2	9/10	83	91	103	0.91	0.74	0.71	0.431
	3	11/1/2017 9:21:33 AM	5000-6509	R1	8/10	81	92	96	0.91	0.73	0.71	0.432
	4	5/30/2018 10:15:01 AM	5000-6509	R2	10/10	79	86	96	0.96	0.74	0.72	0.444
	5	1/30/2019 9:16:04 AM	5000-6509	R1	8/10	77	85	91	0.93	0.73	0.72	0.450
	6	9/11/2019 3:33:20 PM	5000-6509	R2	7/10	74	81	90	0.89	0.76	0.72	0.461
Current:	7	11/7/2019 12:15:53 PM	5000-6509	R1	7/10	74	77	88	0.87	0.75	0.76	0.459

Figure 3.

Example of a GPA report (Carl Zeiss Meditec, Dublin, California) of a glaucomatous eye that has shown progression in peripapillary RNFL thickness (format modified for publication). The deviation map (①) shows areas of change that are statistically significant for the first time (*orange*) and subsequent areas of statistically significant change (*red*). The location and shape of these areas of change indicate the likelihood that the RNFL thinning actually represents glaucoma and its progression. In other words, if the location and shape are consistent with glaucoma, then it is likely that the detected changes are due to glaucoma. Below the deviation maps, graphs show the average RNFL, the superior RNFL, and the inferior RNFL thicknesses over time (②). Again, the first statistically significant drop in RNFL thickness is indicated by an orange dot, and subsequent significant reductions are indicated by red dots. These are trend analyses, as opposed to the event analyses shown in the deviation maps. The average cup-to-disc ratio graph indicates whether there is a

statistically significant increase in cup-to-disc ratio. If the RNFL is decreasing and the cup-to-disc ratio is increasing, then this is good corroboratory evidence that the change measured is real. Below these graphs is the RNFL thickness profile (③), on which the baseline profiles (B_1 and B_2) are overlaid on today's visit (C). This is a useful graph in that the locations and degrees of thinning can be seen, and if they are in areas that would be expected to change with glaucoma, then this increases the likelihood that those changes are real glaucomatous changes. The table of RNFL and ONH summary parameters (④) presents the same data shown in panel *a* and highlights statistically significant change in orange and red. Abbreviations: GPA, guided progression analysis; INF, inferior; NAS, nasal; ONH, optic nerve head; RNFL, retinal nerve fiber layer; SS, signal strength; SUP, superior; TEMP, temporal.

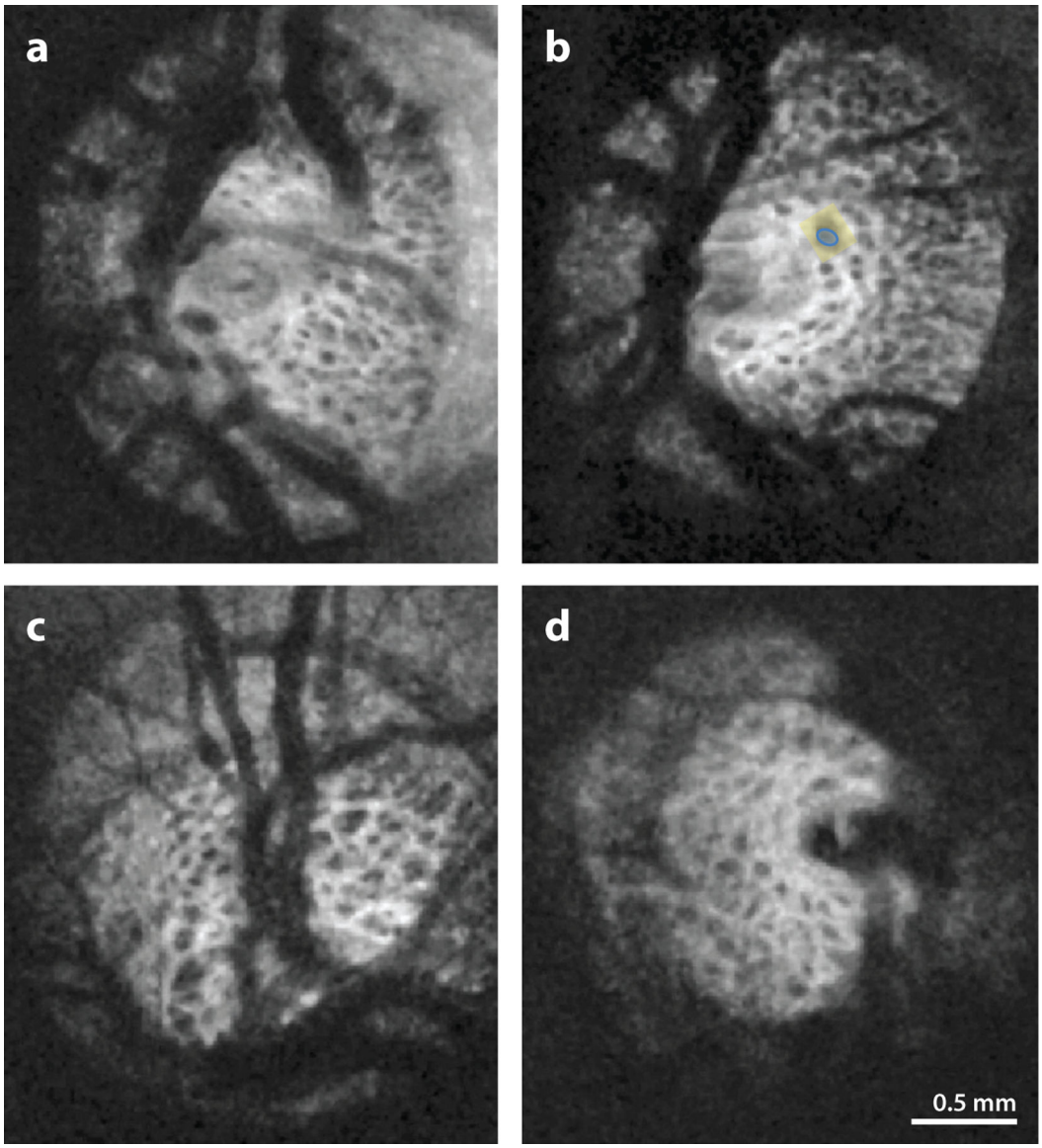

Figure 4.

SS-OCT images displaying the pores (*blue*) and the surrounding beams (*yellow*) in the microstructure of the lamina cribrosa of (*a*,*b*) healthy and (*c*,*d*) glaucomatous eyes. Although the differences in microstructure between glaucomatous and healthy eyes are not visually apparent, using a segmentation analysis that quantifies the microstructure, Wang et al. (2013) found a greater beam thickness–to–pore diameter ratio and greater variability in pore diameter in glaucomatous eyes than in healthy eyes. Figure adapted from Wang et al. (2013); copyright 2013 IOVS, Association for Research in Vision Science. Abbreviation: SS-OCT, swept-source optical coherence tomography.

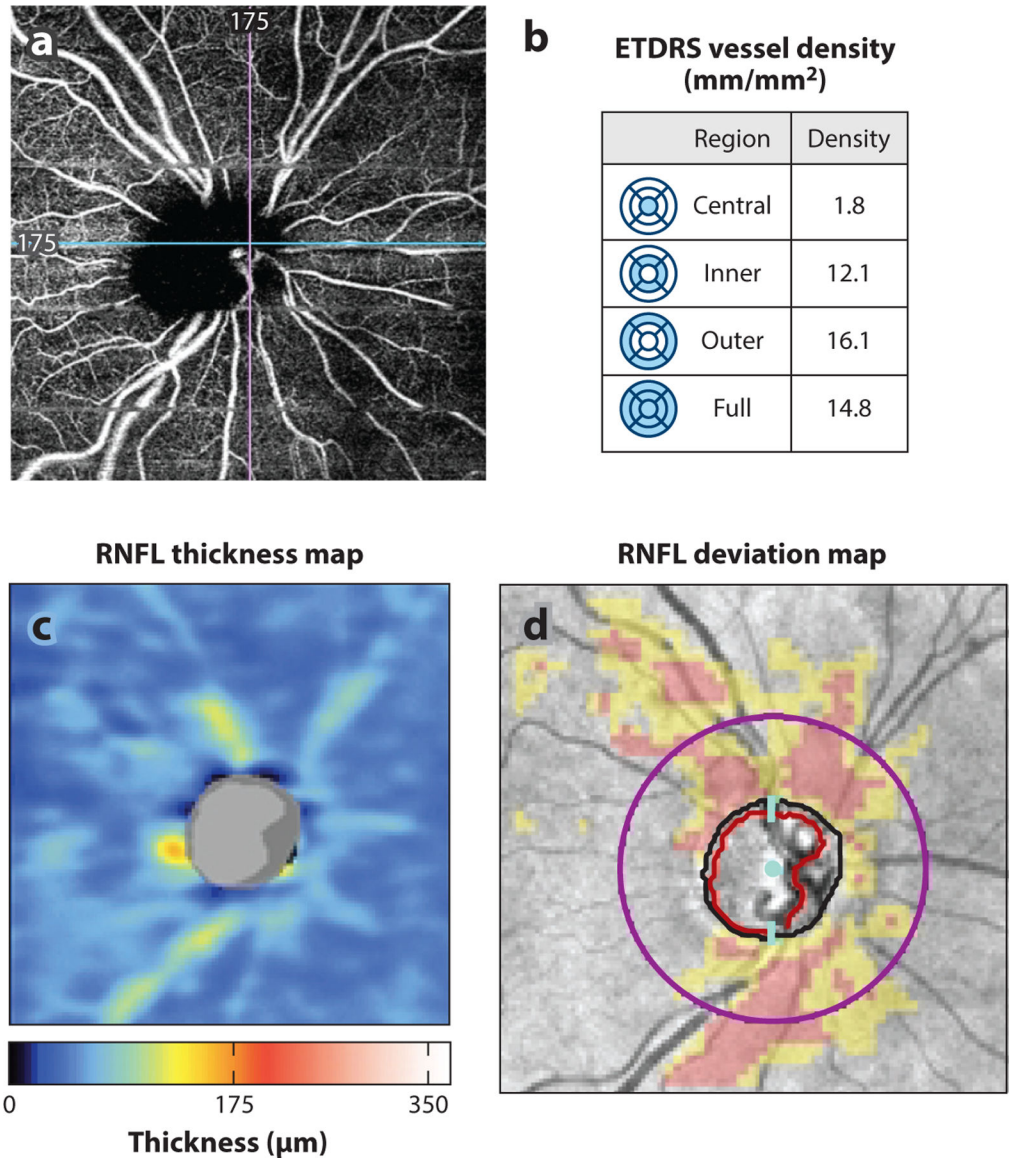

Figure 5.

(*a*) AngioPlex OCT-angiography (Carl Zeiss Meditec, Dublin, California) image of a glaucomatous eye. (*b*) Peripapillary superficial vessel density (mm/mm^2) in the central, inner, outer, and full regions is quantified in the table. (*c*,*d*) Region of decreased vessel density correlates with region of RNFL thinning as seen on (*c*) the RNFL thickness map and (*d*) the RNFL deviation map from the Cirrus HD-OCT (Carl Zeiss Meditec) report. Abbreviations: ETDRS, Early Treatment Diabetic Retinopathy Study; HD-OCT, high-definition OCT; OCT, optical coherence tomography; RNFL, retinal nerve fiber layer.

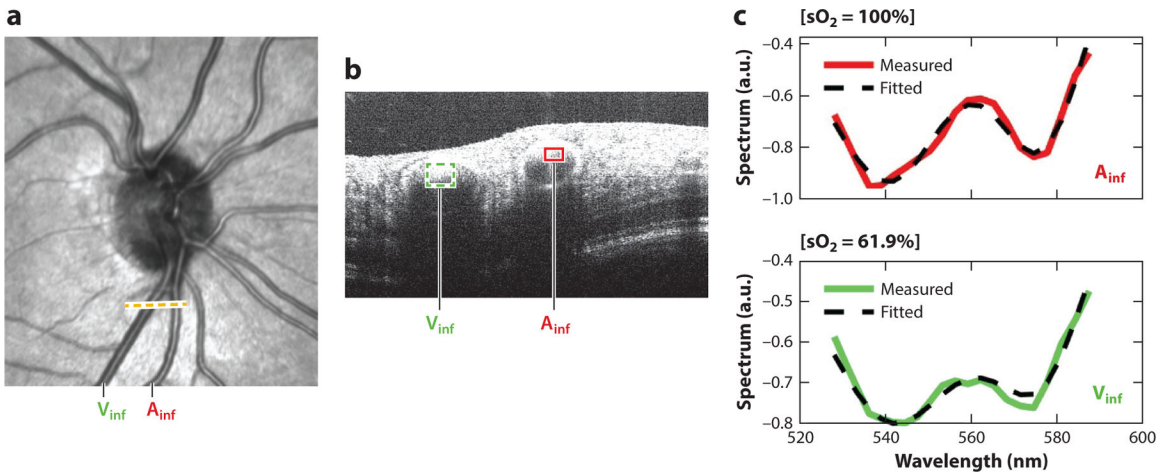

Figure 6.

The artery (A_{inf}) and vein (V_{inf}) at the dotted line on the (*a*) en face visible-light OCT image are seen in the (*b*) B-scan, from which (*c*) their respective spectroscopic OCT signals are fitted to the hemoglobin absorption profile to determine retinal arterial and venous blood oxygen saturations. Image courtesy of Z. Ghassabi, M. Wu, I. Rubinoff, Y. Wang, B. Davis, B. Tayebi, G. Wollstein, J. Schuman, H. Zhang & H. Ishikawa (unpublished study). Abbreviation: OCT, optical coherence tomography.

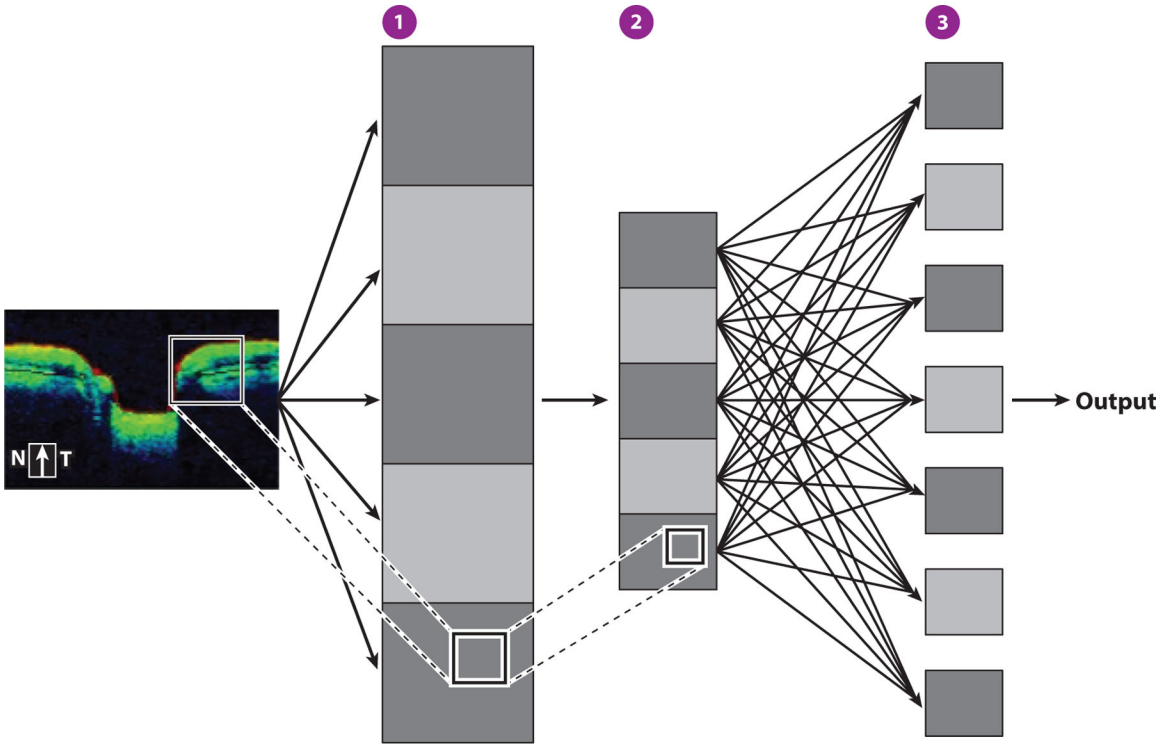

Figure 7.

Convolutional neural networks. Filter functions reduce a portion of the depicted input image (*box*) into feature maps (*gray squares*), which are representations of the presence of features in the input image (①). Pooling layers downscale feature information by summarizing parts of the feature map (②). Forward feeding of information to subsequent layers produces the final output layer, which ultimately yields the desired classification (③). Abbreviations: N, nasal; T, temporal.